UNIVERSITY *of the*
WESTERN CAPE

High-grade metamorphism, anatexis and deformation of metasedimentary rocks from the Kamiesberg Group near Kliprand, southern Bushmanland Domain, Namaqua Metamorphic Province

by

AIDAN LEETZ

3439680

THESIS

Presented in fulfillment of the requirements for the degree of Master of Science

in the

FACULTY OF NATURAL SCIENCES of the UNIVERSITY OF THE WESTERN CAPE

SOUTH AFRICA

Supervisors: Dr. J. Reinhardt

Prof. R. Bailie

2022

Declaration

I hereby declare that this thesis submitted for the degree of Master of Sciences to the Faculty of Natural Sciences at the University of the Western Cape, apart from the guidance of Dr J. Reinhardt and Prof. R. Bailie, it is my own work has not been previously submitted either entirely or partly to any other university or institution of higher education for obtaining a qualification.

Aidan Leetz

Date: 22 April 2022 **Place:** Bellville, Cape Town

Acknowledgements

This research was supported by the Department of Earth Sciences at the University of the Western Cape. I would like to especially thank my supervisor and co-supervisor from the above mentioned department namely; Dr Juergen Reinhardt and Prof. Russell Bailie, whose guidance and insight greatly assisted in the completion of this thesis. The Council for Geoscience and the National Research Foundation (Grant: 110772) are acknowledged for the funding they provided which allowed me to complete this degree. I thank my family for their unconditional support throughout the duration of this study. I also thank my colleagues for their support as well as for sharing their knowledge, insight and skills which all together assisted in the completion of this thesis.

Abstract

Migmatitic metapelites of the Kamiesberg Group are distributed throughout the central Bushmanland Domain (Namaqua Metamorphic Province) which is otherwise dominated by felsic gneisses. This study focusses on an outcrop of migmatitic metapelites situated a few kilometres south-west of the hamlet of Kliprand (Western Cape). The migmatites in this outcrop display the leucosomes and melanosomes as alternating domains that show a fairly regular distribution at the hand specimen scale, without clear evidence for a larger melt accumulation or channels along which melt would have been extracted. This allows the study to investigate the precise genetic relationship between the melt and the associated melanosome, which is often difficult to do due to the mobility of the melt, and the difficulty in tracking the extent of melt extraction at the site of anatexis, and potentially associated melt differentiation. This study aims to investigate the chemical and physical processes during anataxis, and attempts to answer the question whether the present leucosomes represent in-situ melt, or externally derived melt. The distribution of leucosomes in outcrop tends to suggest the former, which was the ultimate reason to conduct the study in this particular location.

The outcrop is located in the region of highest metamorphic grade within the Bushmanland Domain, where peak temperatures and pressures reached between ~750- 870°C and 4.5 – 6kbar respectively. Granulite facies metamorphism brought about incipient partial melting through the biotite dehydration melting reaction: Sillimanite + biotite + quartz → cordierite + garnet + K-feldspar + melt. This resulted in the formation of quartzo-feldspathic, garnet-bearing leucosomes and residual melanosomes which are dominantly comprised of cordierite, sillimanite and K – feldspar with biotite. These two segregations exist side-by-side in the bulk rock as alternating layers parallel to each other and to the main regional fabric, which produces the characteristic stromatic appearance. The leucosomes and melanosomes exhibit similar proportions across the sample set and are also similar in volume to each other. Leucosomes are strain free and host large porphyroblastic garnet grains. Melanosomes contain aligned sillimanite and biotite and make up the matrix in which the leucosomes are hosted.

Leucosomes and melanosomes from each sample were physically separated and analysed for whole-rock major and trace element geochemistry. A bulk rock portion, comprising both the leucosome and melanosome, was also analysed for whole-rock major and trace element

geochemistry. These analyses provide evidence for a pelitic origin. The leucosomes have compositions similar to syeno-granites, whilst the melanosomes exhibit more residual (melt depleted) compositions. These two compositions combine to form a bulk migmatite of pelitic composition. Within the migmatite system elements distribute themselves at favourable sites, with the major element distribution between the leucosomes and melanosomes are controlled by the position of the main phases within the system. Distribution of the major and trace elements between each segregation is typically complementary, whereby, if a certain element is enriched in a particular segregation, it is typically depleted in the opposing segregation. Where an element is evenly distributed between, or has no strong preference for either the leucosome or melanosome, there are typically phases in either segregation competing for the element's distribution. The trace element distribution patterns between the leucosome and melanosome reflect element partitioning between the phases present during peak and post-peak conditions.

At post-peak conditions, the fabric-parallel leucosomes crystallised at their site of formation within the melanosome matrix. There was no significant loss of magma nor was magma derived from an external source. The analysis of a single cross-cutting vein-type leucosome, however, provides an example of a geochemically distinct, externally derived melt fraction.

Table of Contents

List of Figures

List of Tables

1. Introduction

The Namaqua-Natal Province (NNP) hosts igneous and metamorphic lithologies and is divided into two sectors. These are the Namaqua sector in the west and the Natal sector in the east (Cornell et al., 2006). The study area lies just outside the hamlet of Kliprand, Western Cape, within the Namaqua sector, which is composed of five distinct domains. The Richtersveld domain is the western-most segment of the Namaqua sector followed by the Bushmanland Domain then the Kakamas, Areachap and Kheis domains as one progresses further eastwards towards the Kaapvaal Craton (Macey et al., 2018). The study area is located within the Bushmanland Domain (Figure 1). The Bushmanland Domain hosts a symmetrical pattern of roughly east-west trending metamorphic zones. These zones reflect an increase in metamorphic grade towards the centre of the Bushmanland Domain, starting with amphibolite facies in the northern- and southern-most regions increasing to granulite facies in its centre. The granulite-amphibolite facies boundary is characterized by the occurrence of partial melts. Within the granulite facies zone the region of highest metamorphic grade is referred to as upper granulite, which is characterized by the presence of hercynite + quartz (Waters, 1986). The lithologies of interest to this study are situated within this upper granulite facies region. These are hercynite-bearing migmatites.

Migmatites are a product of the partial melting process (Sawyer, 2008). In migmatites, evidence of this partial melting is represented by what is referred to as a leucosome, which is the light-coloured segregation consisting of dominantly quartz and feldspar. This study uses the term ‘‘leucosome’’ to refer to crystallized melt plus entrained phases that cannot be physically separated for bulk leucosome analysis. The melanosome is the dark-coloured residuum which forms as a result of the partial or complete separation of the melt component (now leucosome) to accumulate in patches or layers. The leucosome can remain in its original place of formation (in-situ leucosome) or melt can migrate elsewhere and be emplaced as a leucocratic vein or vein-type leucosome (Sawyer, 2008). This study primarily aims to investigate the precise genetic relationship between the melt and the associated melanosome and to understand the processes involved during anatexis. This includes the melting reactions, melt separation and related geochemical differentiation processes as well as the mechanical behaviour of leucosomes vs residuum during syn-metamorphic deformation. The distribution of leucosomes in outcrop could be an indication of in-situ preservation of the melt product from anatexis. Objectively, this would be accomplished by

microscopic - petrographic and geochemical analyses of the leucosomes, melanosomes and bulk migmatite samples (leucosome plus melanosome).

2. Geological Setting

2.1 Namaqua-Natal Province

This metamorphic belt is 1400km long and 400km wide (Cornell et al., 2006) and borders the Kaapvaal Craton (Figure 1). It is composed of igneous and metamorphic lithologies that were formed and metamorphosed during the 1200-1000Ma Namaqua Orogeny which is associated with the assembly of the supercontinent Rodinia (Dewey et al., 2006). The belt can be divided into two sectors, namely the Namaqua sector in the west (Figure 1) and the Natal sector in the east, according to the two principal regions of exposure of this orogenic belt.

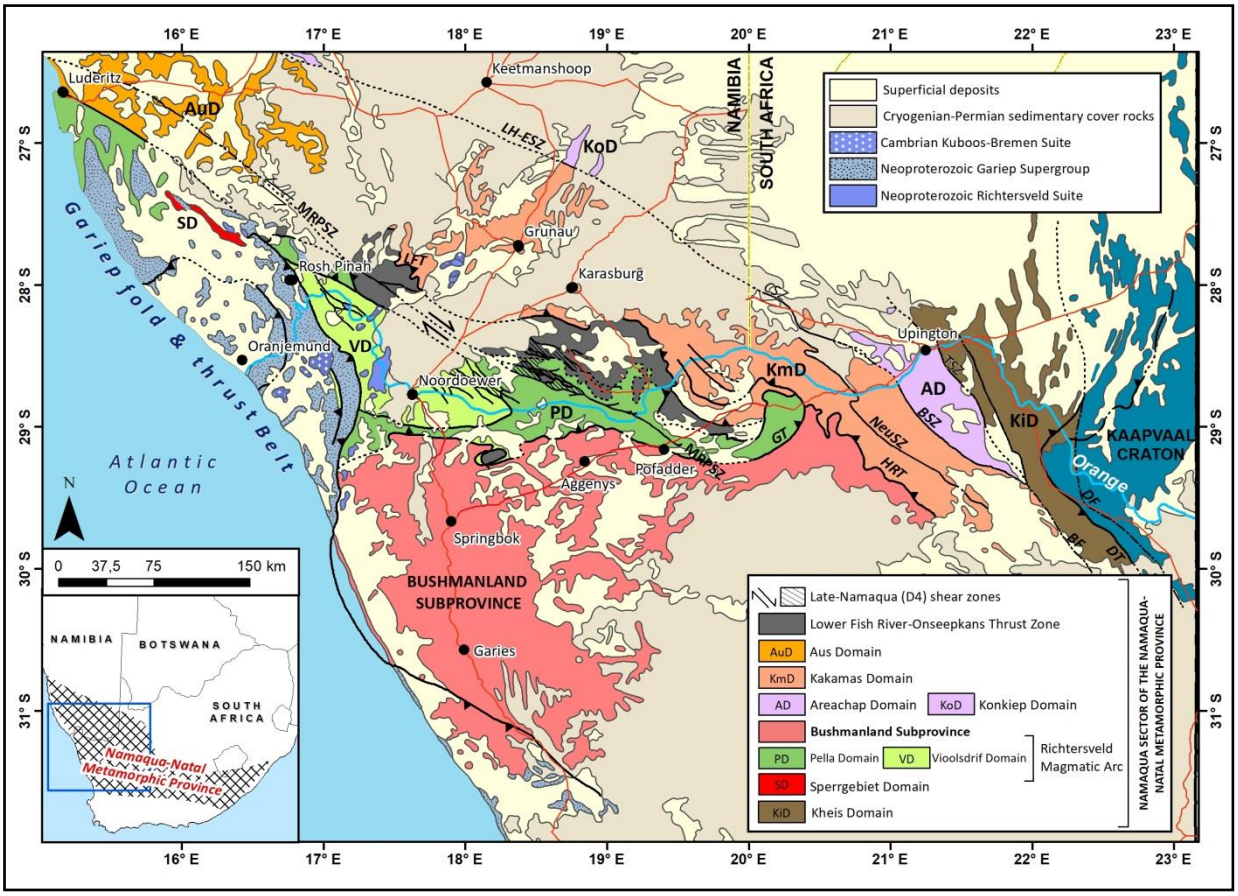

Figure 1: *Regional tectonostratigraphic map of the Namaqua sector of the Namaqua-Natal Metamorphic Belt. Namaqua-age shear zones and thrusts: Lord Hill-Excelsior Shear Zone (LH-ESZ), Kêrelbad Thrust (KbT), Yas Shear Zone (Y), Narries Shear zone (N), Hartebees Rivier Thrust (HRT), Onseepkans Thrust (OT), Lower Fish River Thrust (LFT), Groothoek Thrust (GT), Marshall Rocks-Pofadder Shear Zone (MRPSZ), Sperlingsputs Shear Zones (SSZ), Eureka Shear Zone (ESZ), Cnydas Shear Zone (CSZ), Neusspruit shear zone (NeuSZ), Boven Rugzeer Shear Zone (BSZ), Trooilapspan Shear Zone (TSZ), Brakbosch fault (BF), Doornberg Fault (DF), Dabep Thrust (DT). Pan African thrusts, shear zones and faults: Gemsbokvlei Thrust (GeT); Schakalsberg Thrust (ScT), Steenbok Shear Zone (SbS). After Nke et al. (2020).*

The focus of this study is on the Namaqua Metamorphic Province (Figure 1), located in the northwestern portion of South Africa and bordered by the Gariep Belt to the west and the Kaapvaal Craton to the east (Cornell et al., 2006). The Namaqua Sector can be divided into five distinct domains, which are, from west to east, the Richtersveld Magmatic Arc, the Bushmanland Domain, the Kakamas Domain, the Areachap Domain, and the Kheis Domain (Nke et al., 2020; Figure 1). The term "Domain" as used in Bailie et al. (2019) is used preferentially to the term "Terrane" and "Subprovince" as used by previous authors.

The Richtersveld Magmatic Arc is composed primarily of the volcanic rocks (full spectrum of basalt to rhyolite) of the Orange River Group, along with the sparse hypabyssal and voluminous plutonic rocks (full spectrum of granite to gabbro) of the Vioolsdrift Suite and their metamorphosed equivalents (Blignault, 1977; Reid, 1977, 1997; Reid et al., 1987; Macey et al., 2017). These lithologies are calc – alkaline in nature and are thrust over the Bushmanland Domain (Eglington, 2006).

The Kakamas Domain is bound between the Boven-Rugzeer Shear Zone (BRSZ) to the east and the Hartbees River Thrust to the west (Cornell et al., 2006) and is composed of ~1.2Ga granulite facies supracrustal rocks as well as intrusive granitic lithologies which are related to early and late Namaquan magmatic events (Pettersson et al., 2009), which have ages ranging from 1.21 Ga to 1.08 Ga (Macey et al., 2018).

The Areachap Domain, which borders the Kakamas Domain along the Boven Rugzeer Shear Zone, and bound to the east by the Brakbosch Shear Zone (Cornell et al., 2006), is composed predominantly of 1.30 - 1.22 Ga arc-generated amphibolite facies metamafic and intermediate ortho- and paragneisses as well as 1.21 – 1.08Ga granitic intrusions (Geringer et al., 1994, Cornell and Pettersson, 2007, Macey et al., 2018).

The Brakbosch-Trooilapspan Shear Zone acts as the western boundary of the Kheis Domain which is composed of rocks belonging to the Kheis Supergroup, these include: psammitic rocks, shales, schists as well as metaconglomerates and volcanic rocks. It is middle Paleoproterozoic to late Mezoproterozoic in age and straddles the Kaapvaal Craton along the Blackridge thrust (van Niekerk and Beukes, 2019).

The Bushmanland Domain (Figure 2) hosts the Kamiesberg Group rocks studied in this project and is by far the largest domain, encompassing an area of approximately 60 000 km^2 (Bailie et al., 2019). It is the most westerly (Nke et al., 2020) of the tectonostratigraphic domains of the Namaqua Natal Metamorphic belt being dominated by Mezoproterozoic rocks (Nke et al., 2020).

The Bushmanland Domain had previously been divided into two distinct terranes separated by the ENE – WSW Buffels River Shear (BRS), namely, the Okiep (north of the BRS) and Garies (south of the BRS) Terranes (Eglington, 2006). This concept seems to have fallen out of favour in more recent publications (see Macey et al., 2017 and 2018). Macey et al. (2018) describes the Bushmanland Domain as having a north – western region dominated by 1.85 Ga granitic gneisses and migmatites, recently referred to as the Steinkopf Domain (Nke et al., 2020), whereas the rest of the Bushmanland Domain is dominated by large volumes of both pre- and post-tectonic Mezoproterozoic granitoids.

These include the pre-tectonic Little Namaqualand Suite (~1.21–1.18 Ga), which are the oldest orthogneisses, consisting of strongly foliated granitic augen gneisses (Macey et al. 2018, Bailie et al., 2019). This lithological unit was intruded by the late- to post- tectonic (~1.10–1.03 Ga) Spektakel Suite which is largely comprised of megacrystic granites, granodiorites and charnockites (Bailie et al., 2019). Mafic lithologies in the Bushmanland Domain are limited to two suites, namely, the Oorkraal Suite and the Koperberg Suite (Bailie et al., 2019). The Oorkraal Suite represents a group of deformed and metamorphosed pre-tectonic mafic rocks which include two pyroxene granulites as well as melanocratic to mesocratic biotite-bearing amphibolites (Bailie et al., 2019), whilst the Koperberg Suite represents a group of post-tectonic mafic to intermediate rocks, which are dominantly melanocratic noritoids (Macey et al., 2011). The Bushmanland Domain also hosts pink quartzo-feldspathic gneisses which have unclear protoliths. This lithological unit is referred to as the Lekkerdrink Gneiss (Macey et al., 2011). Garnet-quartz-feldspar leucosomes that have segregated from their source regions, and are fairly voluminous, are present in the region as well and are referred to as the Ibequas Granite (Macey et al., 2011).

Belts of high-grade paragneisses are scattered within these large volumes of granites and are divided into the Bushmanland and Kamiesberg Groups (Macey et al., 2018). The Bushmanland

Group consists of such paragneisses (Macey et al., 2018) as well as quartzites, calc-silicate rocks, amphibolites and Pb-Zn-Cu-Ag massive sulphide mineralization (Robb et al., 1999, Bailie et al., 2007). According to Bailie et al. (2019), the Bushmanland Group is derived from reworked crustal sources which are primarily Paleoproterozoic in age.

The Kamiesberg Group is comprised of metapelitic gneisses, semi-pelitic gneisses, calc-silicates, metaquartzitic rocks and heterogenous migmatitic grey biotite-quartz-feldspar gneisses (Macey et al., 2011). It is possible that the Kamiesberg Group may have originated from the erosion of the Little Namaqualand Suite (Bailie et al., 2019).

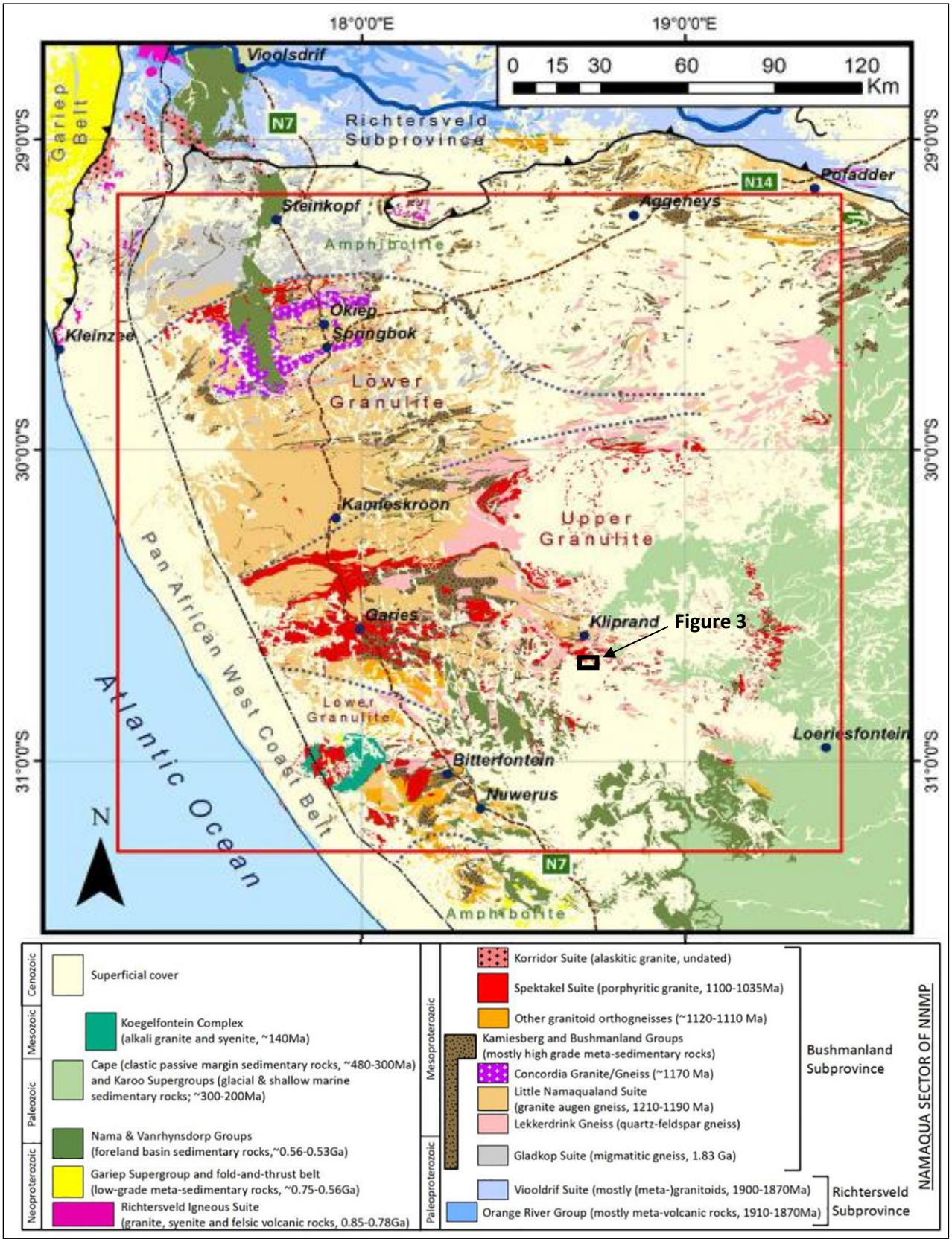

Figure 2: *Geology of the Bushmanland Domain. Modified after the 1:250 000 scale geological maps of the Council for Geoscience. Metamorphic isograds (blue dotted lines) taken from Waters (1986) and Macey et al. (2018). The red square outlined in this map has no relevance to this work and is from earlier work from which the diagram was taken. The black square represents the area outlined in Figure 3.*

Metapelitic gneisses of the Kamiesberg Group occur either as large bodies of pure pelitic composition, elongated regional fabric-parallel bodies in association with other supracrustal units, as well as small xenolith rafts within the late-tectonic granites. The gneisses are commonly migmatitic and exhibit a stromatic texture characterized by bands of melanosomes commonly interlayered with leucocratic leucosomes. These stromatic leucosomes developed through late- to post-tectonic granulite facies melting reactions (Macey et al., 2011). This lithodemic unit also includes bodies of Mg-Al-rich cordierite gneisses referred to as magnesian gneisses (Macey et al., 2011).

The most common supracrustal rock type of the Kamiesberg Group is the banded migmatitic semi-pelitic gneisses. These migmatites are commonly interlayered with other supracrustal gneisses and are characterized by regional foliation-parallel magmatic banding. This lithology contains both concordant and discordant granitoid layers which owe their origin to the dehydration melting of the semi-pelitic gneisses (Macey et al., 2011).

Quartzite are relatively uncommon and occur as lenses parallel to the regional fabric in addition to occurring as discontinuous bodies within the other gneisses. The quartzites are further subdivided into four entities which include the feldspathic quartzites, glassy quartzites, ferruginous quartzites and the graphitic quartzites. (Macey et al., 2011)

Like the quartzites the calc-silicate gneisses are relatively uncommon. These rocks occur as discontinuous bodies within the other gneisses, typically the pelitic and semi-pelitic gneisses (Macey et al., 2011).

The grey migmatite biotite-quartz-feldspar gneiss occur as compositionally banded bodies that are predominantly biotite ± orthopyroxene-quartz-feldspar gneisses but include layers of the other Kamiesberg Group lithologies (pelites, semi-pelites, calc-silicates, quartzites) (Macey et al., 2011).

2.2 Deformation

Five phases of deformation are recognized within the Namaqua-Natal Province (D_1 – D_5). The first deformational event (D_1) is Paleoproterozoic in age and related to the 1905 – 1865 Ma Orange River Orogeny. The second (D_2) to fourth (D_4) are Mesoproterozoic to Neoproterozoic in age (1230 - 950 Ma), and are related to the Namaquan Orogeny. The fifth deformational event (D_5) is related to the Pan-African Gariep Orogeny and has a Late Neoproterozoic to Cambrian age (Diener et al., 2017).

According to Miller (2012) and references therein, D_2, an accretionary and collisional event, is considered the main deformational event preserved in the Bushmanland Domain with an age ranging from ~1.13 to ~1.06 Ga. This produced isoclinal recumbent folds and is represented by an S_2 foliation which is visible in the Little Namaqualand Suite. Peak prograde metamorphism (M_2) occurred at ~1.03 Ga and was related to peak D_2 deformation (Raith et al., 2003). D_3, according to Macey et al. (2011) and authors therein, deformation is characterized by E-W trending folding (F_3) which produced upright to inclined shallow-plunging open folds, whilst, S_3 can be described as a non–penetrative, discrete sub–vertical cleavage. This cleavage is observed almost exclusively in the augen-gneiss units of the Little Namaqualand Suite. D_4 resulted in the folding of existing structures to form N-W trending open folds, producing no new penetrative foliation. Miller (2012) suggests that D_3 - D_4 occurred between ~1.06 and ~1.04 Ga, synchronous with the second metamorphic peak characterized by low pressure and high- to ultra-high temperature granulite facies metamorphism.

2.3 Metamorphism

The Bushmanland Domain displays a pattern of metamorphic zonation (Figure 2) beginning with upper amphibolite zones in the northern and southern parts. In metapelites, these zones are characterized by the mineral assemblage: garnet + cordierite + K–feldspar. The metamorphic grade increases towards the centre of the Bushmanland Domain to a granulite-facies zone characterized by the pelitic assemblage (Macey et al., 2011):

Quartz – K-feldspar – cordierite - plagioclase – garnet – sillimanite – opaques ± biotite

which was formed by the prograde melting reaction (Waters, 1986):

Sillimanite + biotite + quartz → cordierite + garnet + K-feldspar + melt.

This biotite dehydration reaction marks the transition from upper amphibolite to granulite facies. Within the centre of this zonation pattern is an upper granulite facies sub-zone in which the study area is located; this is the highest-grade zone of the Bushmanland Domain and characterized by the presence of hercynite + quartz (Waters, 1986).

Peak P-T conditions of the upper granulite facies zone are between ~750°- 870°C and 4.5 – 6 kbar (Macey et al., 2018). This highest-grade metamorphism occurred around 1030 Ma and was preceded by amphibolite facies metamorphism (>550°C, ~3.5 kbar) during the main Namaquan orogeny. Much of this record, however, was eradicated by granulite facies metamorphism (Macey et al., 2011, Macey et al., 2018).

3. Methodology

3.1 Sample preparation

Nine migmatite samples were selected for geochemical analysis. They are KL2, 5A, 6, 7, 9, 13, 20, 25 and 26. These samples were collected between 2017 and 2019. Six of these samples (KL 2, 5A, 6, 7, 9 and 26) were selected on the basis of how well the leucosome and melanosome parts were separated physically in the rock as seen in cuts orthogonal to the foliation. From each of these samples, a sufficiently large portion was assigned to bulk rock analysis, while cut slabs were put aside for leucosome and melanosome analysis. In sample 13 the leucosome and melanosome are as distinct as the first batch of samples, but this sample also hosts a vein-type leucosome cutting across the foliation. This vein was cut out from the sample to be analyzed.

The sample portions selected for separate leucosome and melanosome analysis were generally slabs cut orthogonal to the foliation (S) and parallel to the lineation (L). Using a thin saw blade, the leucosome and melanosome parts were initially separated by cutting along the boundary between the two. The irregular prolate shape of the leucosomes made it necessary to make corrective cuts to carefully remove melanosome remains from the leucosome chips and vice versa. In the process, each cut-out rock chip was carefully checked for "purity" of composition. Any parts that did not clearly belong to either melanosome or leucosome along the boundary domains were also removed. Thus, rock chips typically several centimetres long and a few millimetres to about a cm across were obtained. The total weight of the leucosome separates amounts to between 140g and 160g per sample (see Appendix A). The total weight of the melanosome separates amounts to between 58g and 170g per sample (see Appendix A).

Thus, for each sample there is a bulk rock to be processed as well as two separates, a leucosomes portion and a melanosome portion. In total there were twenty-one samples to be analysed, three analysis per six samples for the first batch (KL2, 5A, 6, 7, 9, and 26) and two 'bulk only' samples (KL20 and 25) plus the single vein-type leucosome analysis of KL 13.

All samples were cleaned with deionized water and oven-dried, larger bulk samples were then crushed with a steel jaw crusher to smaller pieces. The leucosome and melanosome separates and the vein-type leucosome fragments were too small for the jaw crusher. Samples were

then put into a weak acidic solution, with the beaker immersed in an ultrasonic water bath to remove any surface contamination. The samples were then again water-cleaned and dried in an oven.

Milling of the samples proceeded with the bulk portions first. Before each sample change a quartz run was carried out, after which the bowl, ring and lid were cleaned with water and alcohol. This process was repeated for the leucosome and melanosome samples as well. A chrome steel milling bowl was used.

All cutting, crushing and milling of samples was carried out at the Department of Earth Sciences at the University of the Western Cape.

3.2 Whole-rock major and trace element analyses

3.2.1 XRF analysis

Major elements for all samples were determined by X-ray fluorescence (XRF) spectrometry on glass beads at Stellenbosch University's Central Analytical Facilities (CAF). 1 g of rock powder was mixed with 10 g of trace element- and REE-free flux (lithium metaborate/tetraborate mixture: ($LiBO_2$ = 32.83%, $Li_2B_4O_7$ = 66.67%, LiI = 0.50%) during the preparation of glass beads. Whole-rock major element data were acquired by X-ray fluorescence spectrometer analysis on a PANalytical Axios Wavelength Dispersive spectrometer fitted with a rhodium tube and LiF200, LiF220, LiF420, PE and PX1 crystals. The instrument is fitted with a gas-flow proportional counter (using a 90% argon and 10% methane gas mixture) and a scintillation detector. Major elements were analyzed on a fused glass disc at 50kV and 50mA tube operating conditions. The control standards used in the calibration for major element analyses were BE-N (basalt reference values), JB-1 (basalt (depleted) reference values), BHVO-1 (basalt reference values), JG-1 (granodiorite reference values) and WITS-G (granite reference values). Loss on ignition (LOI) was calculated by weight difference after ignition to 1000^{o}C.

3.2.2 LA-ICP-MS analysis

The sample preparation procedure for trace elements involved the preparation of the glass discs using an automatic Claisse M4 gas fusion instrument utilizing ultrapure Claisse Flux (66.67% $Li_2B_4O_7$; 32.83% $LiBO_2$; 0.50% LiI) with a sample to flux ratio of 1:20. A Resonetics 193nm laser connected to an Agilent 8800 ICP-MS was used to analyze the trace element

concentration of fused glass discs. Operating conditions for the laser were 8Hz frequency whereby a spot size of 104 μm was created during the laser ablation analysis. Ablation was performed in helium gas at a flow rate of 400 ml/min and mixed with argon before introduction into the plasma. The laser took approximately 25 seconds to warm up and an additional 40 seconds for each spot analysis. Calibration standard NIST 60 was used. Calibration involved sample bracketing every 15 – 20 samples. Certified reference standards BCR or BHVO-1, both basaltic glass, was used for this purpose. At the beginning of each sequence a fusion control standard from certified basaltic reference material (BCR) was analyzed to verify the effective ablation of the fused material. The data were processed using the Iolite v 3.71 software.

4. Petrography

4.1 Field descriptions

The samples were collected from an outcrop approximately 15km south of the settlement of Kliprand. The study area (Figure 3) forms the top part of a hill with its point of highest elevation about 760m above sea level. The total outcrop area is estimated to be an area of 85 000 m².

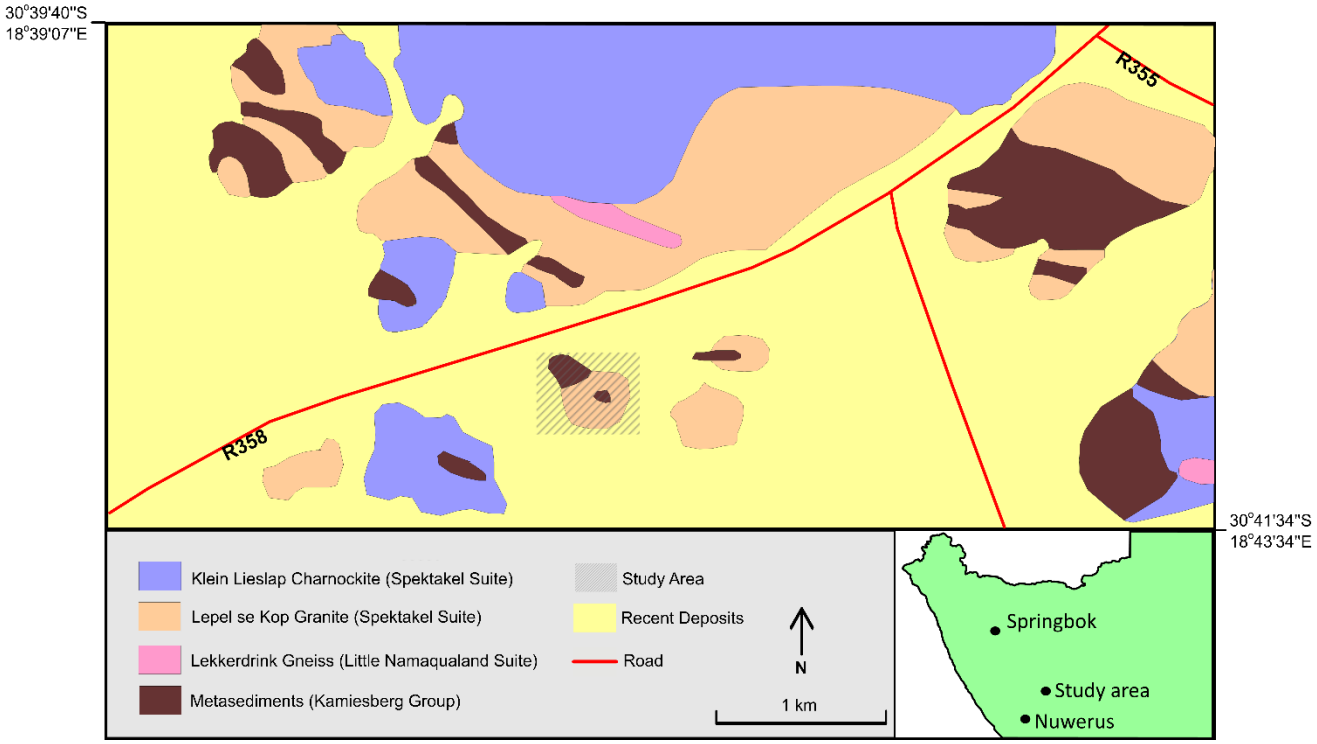

Figure 3: *Lithological map of the study area and surrounding area, modified for this study after Bailie et al. (2019)*

The study area is part of the Namaqua Metamorphic Province, situated in a landscape dominated by gneisses and granites. Lithological units in the nearby surrounds include the Lekkerdrink Gneisses of the Little Namaqualand Suite, Spektakel Suite granites, mafic lithologies of the Oorkraal Suite and the metasedimentary lithologies of the Kamiesberg Group. The study area lies within the Lepel se Kop pluton. The immediate surrounds are made up of this granite as well as the Klein Lieslap Charnockite, both of which belong to the Spektakel Suite. The study area shows exposures of the Lepel se Kop granite. This garnet-bearing, megacrystic granite occurs as massive bodies throughout the region hosting rafts of

metasedimentary material (Figure 3). It exhibits moderately aligned tabular K-feldspar megacrysts (Figure 4A) as well as garnet-rich quartzo-feldspathic segregations. The metasedimentary material (Figures 4B, C and D) hosted by these granites includes lenses of typically off-white feldspathic quartzites which are compositionally banded and exhibit a preferred alignment of biotite.

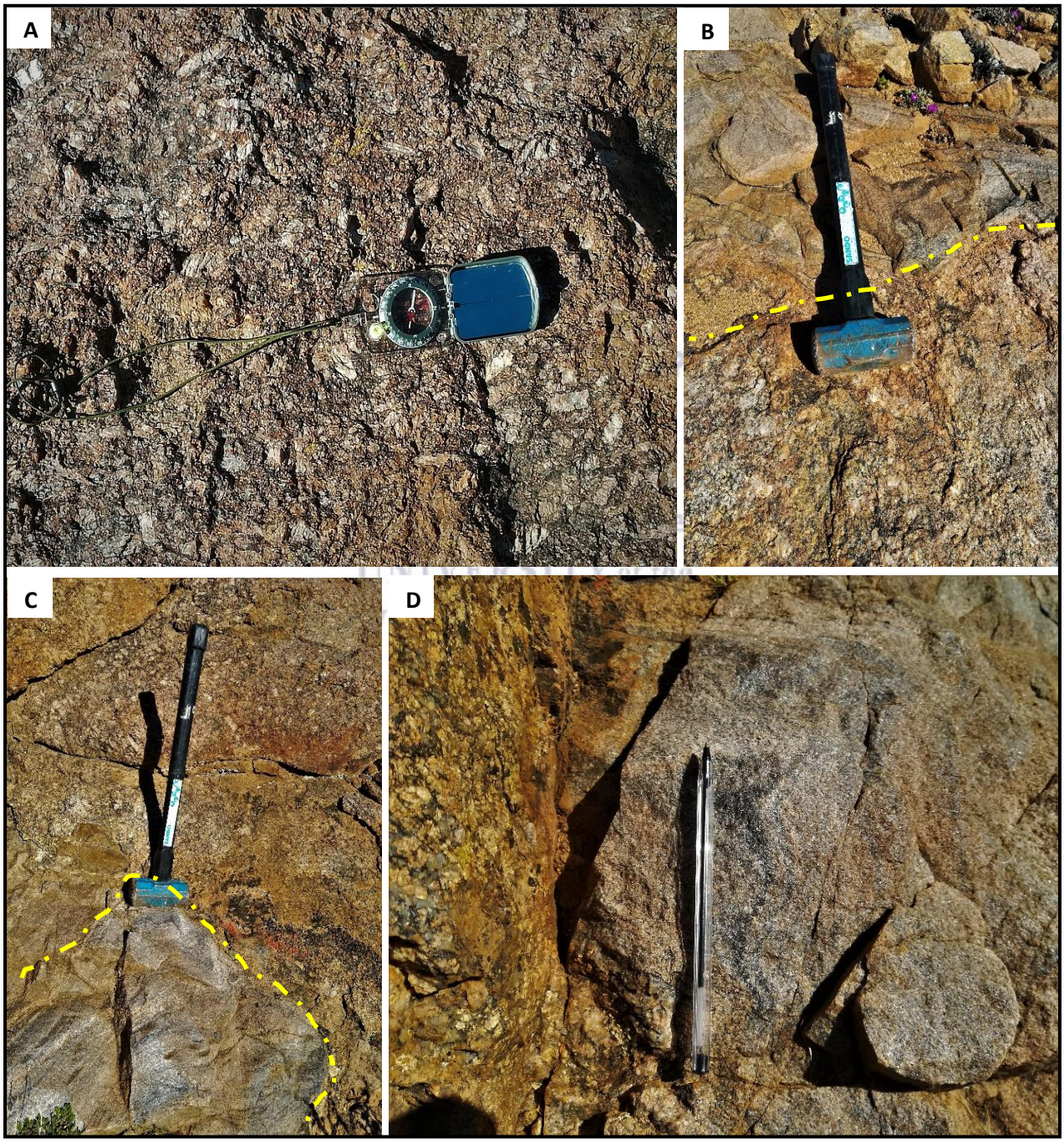

Figure 4: *Other lithologies in the study area.* ***A*** *- Lepel se Kop granite showing feldspar megacrysts.* ***B, C*** *- Contacts between Lepel se Kop granite and metaquartzite of the Kamiesberg Group (outlined by yellow dashed line).* ***D*** *- Close up view of the metaquartzite. All images presented here were taken in the study area outlined in Figure 3.*

Migmatitic metasedimentary rocks are present on this outcrop as well. They are the focus of the study. Evidence of partial melting is displayed here in the form of garnet-bearing, quartzo-feldspathic leucocratic segregations. The outcrop is littered with these migmatite boulders which are up to a metre in size. Typically, boulders display a face in which the constituent segregations are parallel to each other (Figures 5 and 6). The light-coloured segregation is referred to as the leucosome and the darker is referred to as the melanosome. These terms have been defined above. An initial visual inspection across the outcrop indicated that melanosome and leucosome volumetric proportions are roughly equal on average, with local variations of one marginally dominating over the other. The leucosomes define a lineation and display an elongated lens shape; their long axes are all aligned in roughly the same direction. The 3D structure of the leucosomes can be determined in the outcrop from exposures which can be viewed from all sides. Leucosomes from in-situ outcrops display a general strike of E – W to ESE – WSW. The melanosomes (specifically platy minerals therein) define a SW-dipping foliation. These rocks also host leucocratic garnet - bearing veins which cut across the main foliation (Figure 6) and are typically thicker than the fabric parallel leucosomes. Well preserved in situ surfaces are visible in Figure 6 and more weathered boulders are visible in Figure 7.

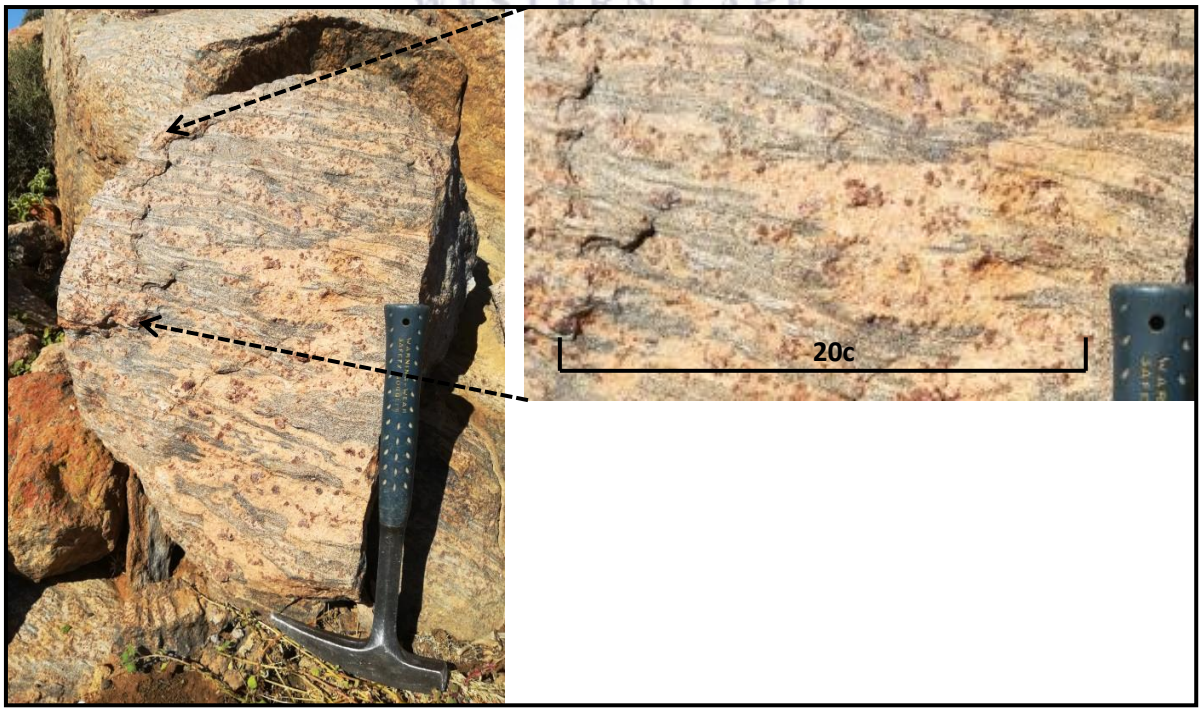

Figure 5: *Typical example of un-weathered migmatitic gneiss illustrating alternating leucosomes and melanosomes. Stromatic texture and spotted appearance apparent. Estwing hammer for scale.*

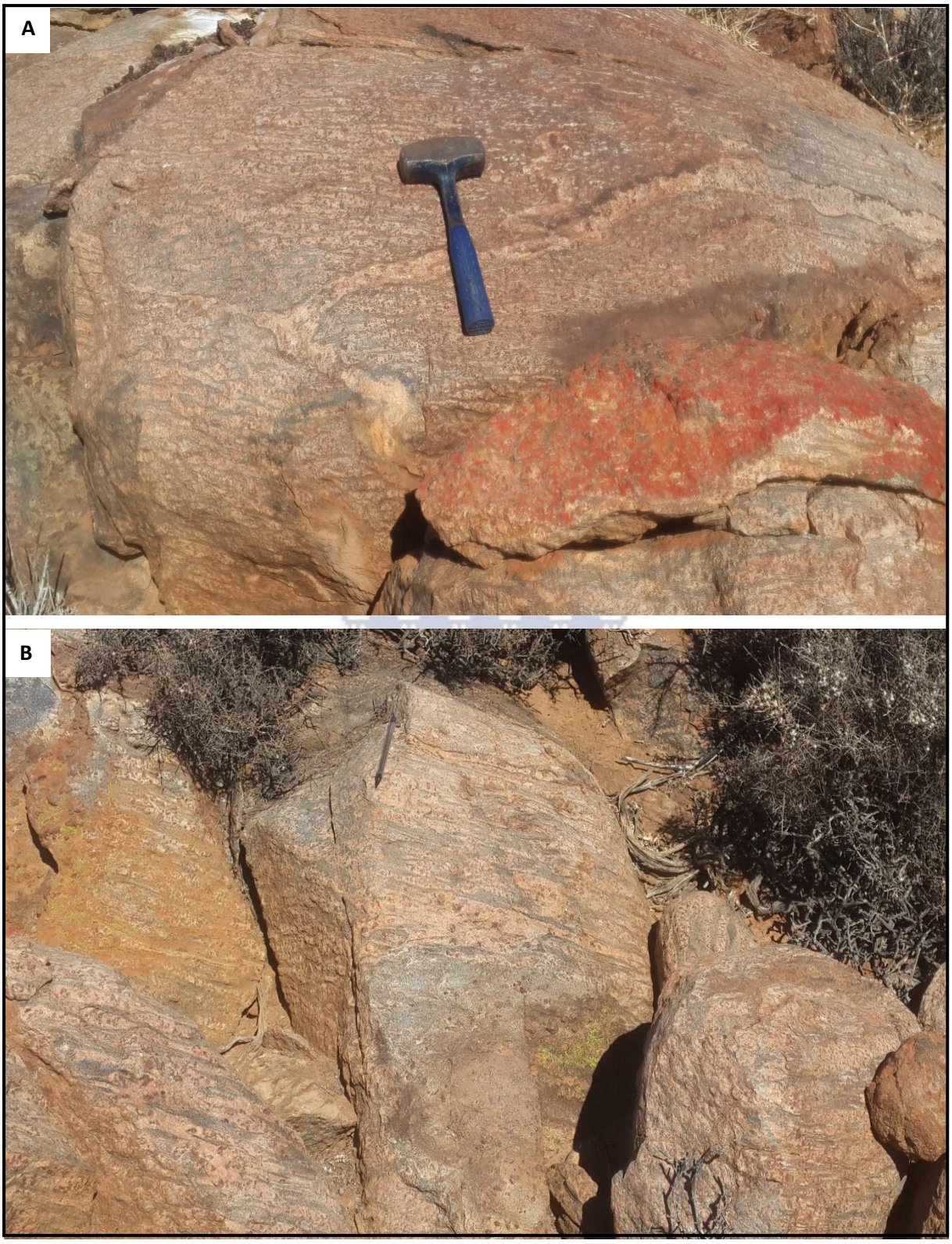

Figure 6: *A - B - Typical examples of in situ migmatite outcrop in the study area. Hammer and pen points north. Vein network visible in A. Alternating layers clearly visible as well as general shared orientation of the fabric-parallel leucosomes.*

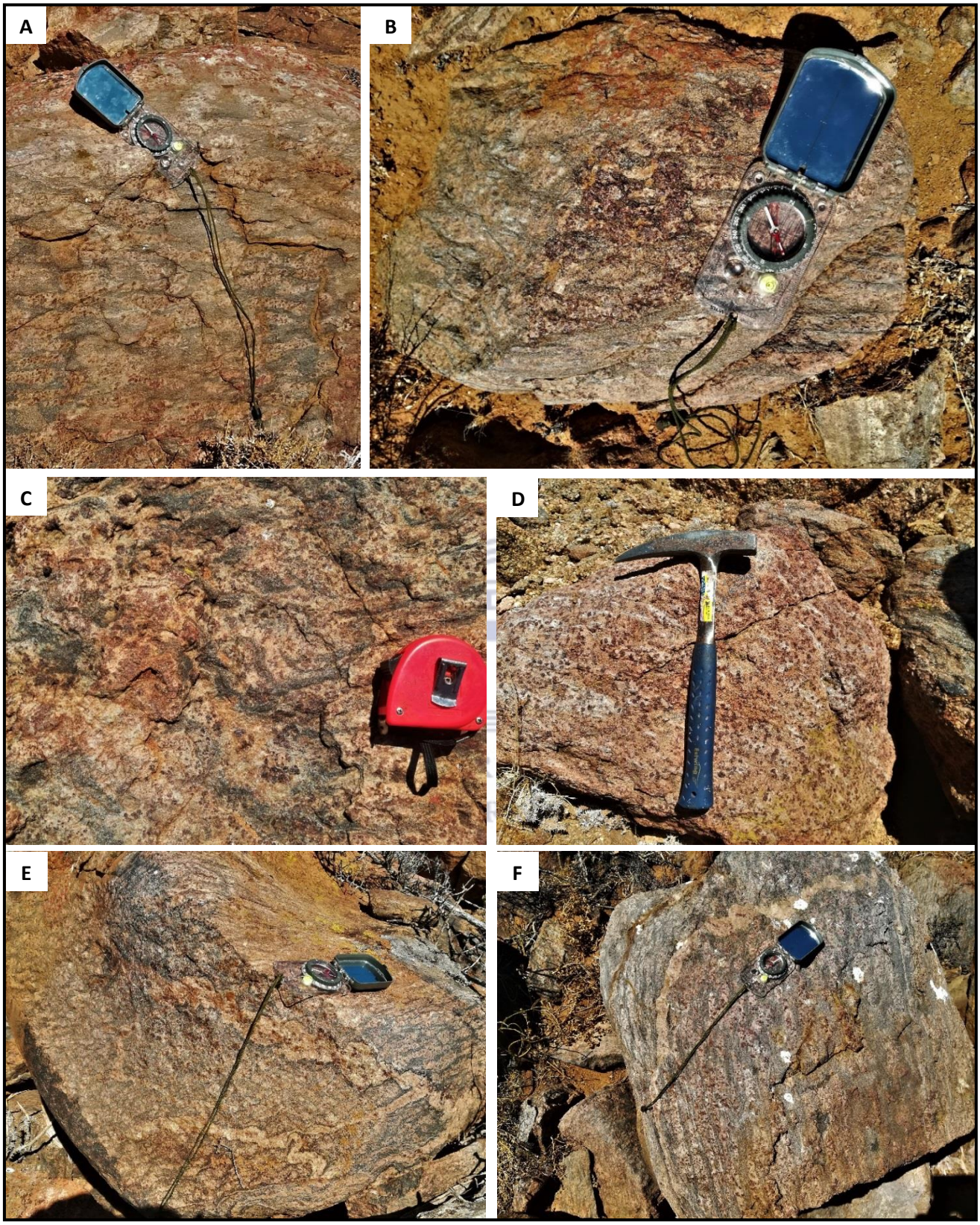

Figure 7: ***A – D****, common weathered appearance of the migmatite boulders, each image showing a different degree of weathering.* ***E*** *and* ***F*** *- vein-type leucosomes.*

The leucosomes (Figures 8 and 9) of the migmatite are typically light brown to orange in colour, dominantly consisting of quartz and K-feldspar. Garnets are present in these layers as well in great abundance and are much coarser than the quartz and feldspar. They often occur in large aggregates. The abundance of garnet crystals gives rise to the spotted appearance of the leucosome. The leucosomes vary in thickness from sample to sample, with thicknesses typically ranging from <10mm to approximately 70mm in width. Garnet clusters are often larger than the rest of the leucosome which causes the leucosome to sometimes appear as if it is bulging along the edges, which in turn causes the appearance of a wave-like shaped edge when viewed in samples cut parallel to the lineation (Figure 7). The leucosome is a linear feature and its shape can be described as elongated lenticular. The long axis of the leucosomes is clearly visible in Figures 8C and D and Figure 9A, B, E and F. In samples cut orthogonal to the lineation, the enclosed nature of the leucosome patches is visible (Figures 8A, B and 9C, D). Having samples cut both parallel and orthogonal to the lineation allows for a detailed analysis of the 3D structure. Typically, the fabric-parallel leucosomes are separated from each other by a width of melanosome, however, there are instances where the leucosomes appear to be connected to each other as a result of the melanosome appearing to terminate between them. As these leucosomes are laterally persistent, occur parallel to the main foliation, and are bordered by melanosome on either side, the texture can be described as stromatic (Sawyer, 2008). A pale grey to– off-white leucosome is also present; this variety contains the same constituent minerals, however, the grey colour is attributed to the presence and abundance of sillimanite as well as significantly larger proportions of quartz. K-feldspar is also visibly less abundant in this type of leucosome (Figure 9A). A vein-type leucosome is present in certain samples. This type of leucosome cross-cuts the main foliation. These vein-type leucosomes usually exhibit folding and are thicker than the other leucosomes. The mineralogical composition of these leucosomes is the same as that of the others. However, the grain size of the minerals is also visibly much coarser (Figure 9C and D).

The leucosomes are set in a matrix of dark minerals. These melanosomes are made up of largely biotite, quartz and sillimanite and exhibit a dark grey to black colour (Figure 8). The constituent minerals are typically finer grained than those of the leucosomes. At the hand specimen scale the alignment of sillimanite is visible and generally occurs as slightly coarser grains orientated parallel to the main regional fabric. The melanosome is a planar feature;

when viewed in a position where it is parallel to the leucosome it occurs as laterally persistent bands the shape of which are determined by surrounding leucosomes. When viewed perpendicularly to the lineation the melanosome occur as a matrix between the leucosome patches (Figures 8B and 9D). Certain samples contain what can be described as layers of quartz and sillimanite (Figures 9E and F). It is an elongated accumulation of quartz and sillimanite which occurs in both the leucosome and melanosome. This is not to be confused with the sillimanite and quartz rich leucosome. Sillimanite is, however, absent from the vein-type leucosomes.

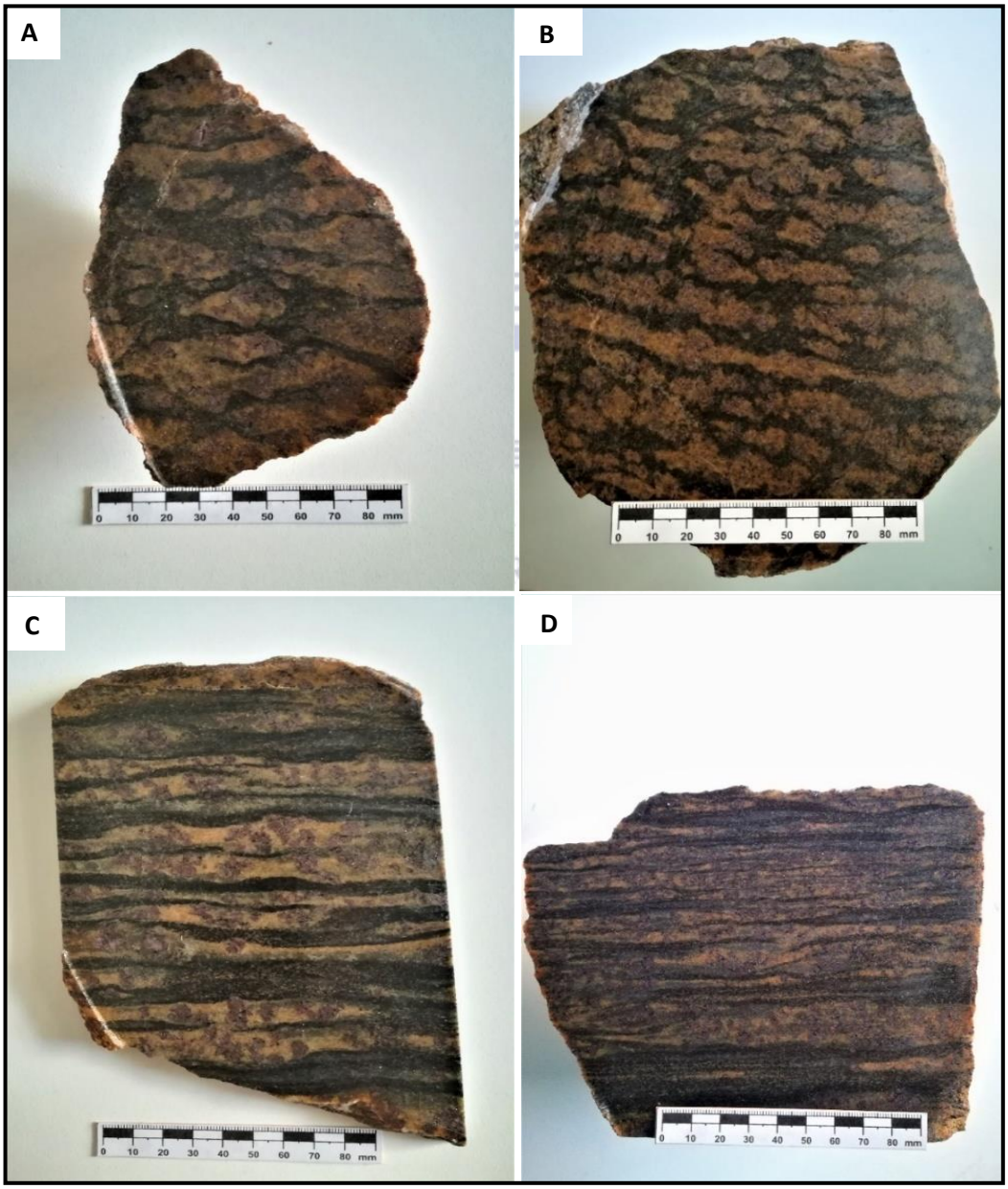

Figure 8: *Cut samples displaying the range in size and distribution of leucosomes.* ***A*** *and* ***B*** *display samples that were cut perpendicular to the lineation.* ***C*** *and* ***D*** *display samples cut parallel to the lineation. The manner in which the garnet clusters affect the shape of the leucosome is best visible in* ***A*** *and C.*

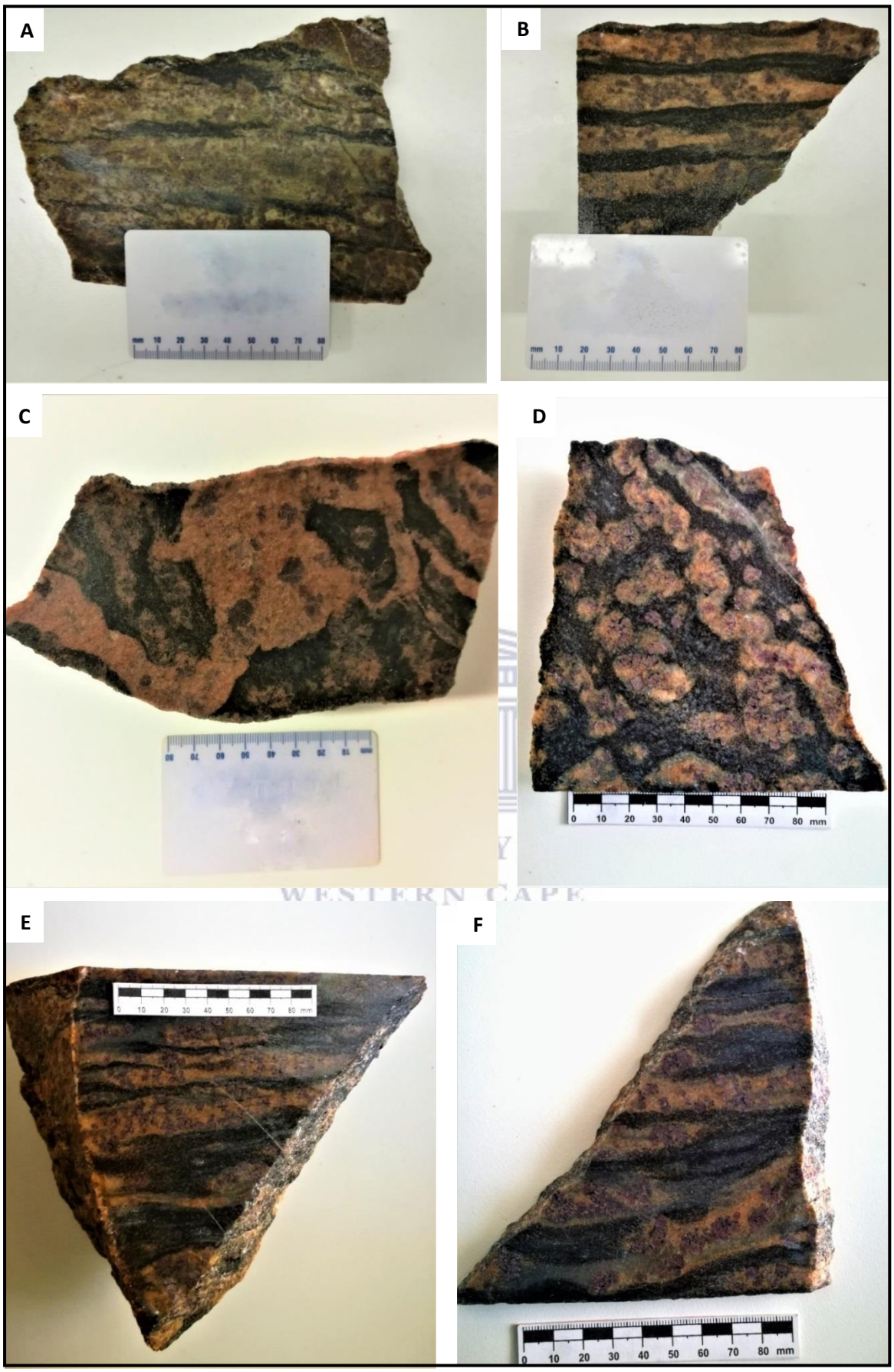

Figure 9: ***A*** *– sample displaying a quartz and sillimanite rich leucosome,* ***B*** *– sample displaying typical quartzo-feldspathic leucosomes (note the difference in colour to that of* ***A****).* ***C*** *and* ***D*** *– display different vein-type leucosomes. The coarser natures of these leucosomes are visible in* ***C*** *whilst folding of this type of leucosome is observed in* ***D****.* ***E*** *and* ***F*** *display aforementioned quartz and sillimanite bands.*

4.2 Microscopic – petrographic analysis

Thirty-two thin sections of migmatite samples were analysed (Table 1). This selection includes all the samples that were analysed geochemically, plus additional ones. All samples from KL 1b to KL 12a show evidence of melanosome and leucosome segregation. Thin sections were prepared from cuts parallel and perpendicular to the linear arrangement of the leucosome patches. Thin sections of samples KL 13 – KL 32 were prepared to study specific features. KL 13 and 32 were prepared in order to study the cross-cutting, coarse-grained vein-type leucosomes, their composition, relationship to the melanosome and their specific characteristics relative to the concordant leucosomes. Thin sections KL 20a through to KL 26e were prepared in order to study leucosomes which are more sillimanite- and quartz-rich. Mineral abundances listed in Table 1 are visual estimates from thin sections, which correspond to the percentage area a mineral occupies in a thin section.

The leucosomes (Figure 10) predominantly contain the minerals garnet, K-feldspar (orthoclase) and quartz which give rise to their light-coloured appearance. Quartz (25 - 40%) grains range in size from 0.05 – 3mm, whereas the size of the orthoclase (25 – 48%) grains vary between 0.1 – 2.7 mm. Orthoclase also exhibits microperthitic exsolution textures. Symplectic intergrowths of quartz and orthoclase are present as well. Plagioclase (8 – 23%) is limited to leucosomes of only two samples. It has grain sizes ranging from 0.2 – 1.75 mm. Furthermore, these leucosomes contain substantial amounts of poikiloblastic subhedral garnet (8 – 35%). Inclusions in these garnets comprise rounded quartz which is the most profuse. Cordierite inclusions are present as well. Biotite occurs as rounded inclusions within the garnet as well as a pseudomorphic grains after garnet. Many of these garnets are relatively rich in opaque minerals with respect to their surrounds. Deformed quartz commonly rims these garnets and is locally accompanied by cordierite. Symplectic intergrowths of quartz and cordierite are relatively common along the borders of the garnet grains. The size of the garnet grains ranges from 0.4 mm to 5.5 mm with aggregates as large as 7 mm present. The abundance of garnets within the leucosomes gives these layers a distinct spotted appearance. Sillimanite (2 – 22%) also occurs in association with garnet in the form of acicular overgrowths (on garnet), however, its presence is not restricted to this form. In certain thin sections sillimanite occurs in association with quartz forming layers which run both parallel and perpendicular to the lineation. There is indeed quite a large spread in terms

of the crystal length of sillimanite which ranges from 0.1 – 5 mm. Other minerals in these sillimanite bands, such as quartz and orthoclase, exhibit significantly smaller grain sizes than that of their counterparts which are not in association with sillimanite. The leucosomes exhibit a relatively noticeable portion (2 - 5%) of opaque minerals (0.025 – 1.1 mm in size).

Samples KL 13 and 32 (Table 1) contain the cross-cutting, vein-type leucosomes (Figures 10e and 10f). They differ from the fabric-parallel leucosomes as they are significantly coarser grained with grain sizes ranging from 0.2 mm – 6 mm for orthoclase and 0.1 mm – 6.25 mm for quartz as opposed to maximum sizes of 2.7 mm and 2.5 mm, respectively for K-feldspar and quartz of the fabric-parallel leucosomes. These veins contain between 38 – 45% quartz and between 40 – 55% K – feldspar. Garnets are also much less abundant in these segregations with abundances between 0 – 15%. Opaque minerals are almost absent here as well, and, if present, they are restricted to in and around the few garnet grains. The only other accessory mineral present in these veins are zircons which are much less abundant than in the fabric-parallel-leucosomes.

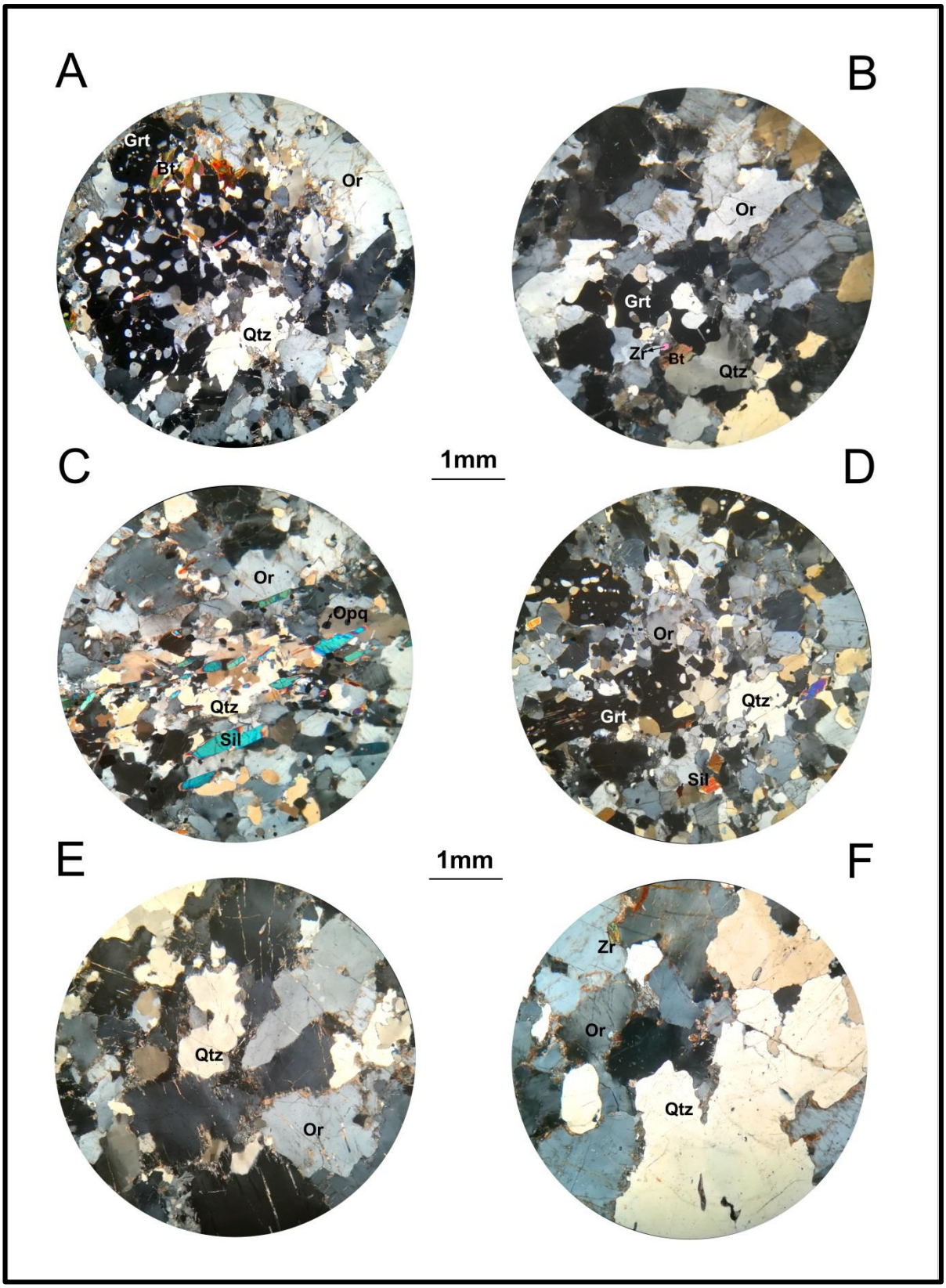

Figure 10: *Photomicrographs of the leucosomes of the sample set in cross polarized light. A – B represents leucosomes without sillimanite. C – D are leucosomes which contain sillimanite. E – F illustrate coarse leucocratic veins. A – KL 1b, B – KL 4b, C – KL23b, D – KL 21, E – KL 32, F – KL 13a. Or – Orthoclase, Grt – Garnet, Bt – Biotite, Qtz – Quartz, Sil – Sillimanite, Opq – Opaque, Zr – Zircon.*

The melanosome segregations (Figures 11a – 11d) are predominantly composed of K-feldspar orthoclase, quartz, biotite and cordierite, with the latter two accounting for the dark colour. Plagioclase is present as well in relatively small quantities (2 - 8%) and restricted to a few samples. Biotite (5 – 20%) grains range in size from 0.05 – 1.75 mm and are typically aligned and help define the main foliation. Quartz (22 – 34%) and orthoclase (18 – 35%) exhibit sizes between 0.05 – 2 mm and 0.1 – 1.6 mm respectively. Orthoclase commonly exhibits sericitic alteration and microperthitic exsolution textures. Cordierite (10 – 35%) exhibits sizes between 0.05 and 1.5 mm and is commonly pinitized, especially along its fractures. Cordierite typically contains rounded quartz as well as opaque inclusions. Sillimanite (2 – 32%) is present as well and displays grain sizes between 0.1 – 6 mm. It occurs in association with quartz and cordierite in the aforementioned bands. The orientation of this sillimanite parallel to the main foliation and lineation gives rise to a nematoblastic texture. Opaque minerals are present in noticeable quantities (2 - 8%) with sizes ranging from 0.025 – 1.1 mm. These melanosome segregations are typically fine- to medium-grained apart from the local coarse sillimanite grain and, on average, exhibit a smaller grain size than of the constituent minerals of the leucosomes. Layers of dominantly quartz and sillimanite occur independently from both the leucosome and melanosome. They contain significantly larger quartz and opaque minerals than the melanosome. Cordierite is present in these layers as well. These layers are easily recognizable as there is a noticeable absence of orthoclase. That being said, the boundary between these layers and the melanosome is easily recognizable in thin section view.

The contact between the leucosome and melanosome can be difficult to define at the grain scale (compared to hand sample). Contact zones between the segregations are displayed in Figure 11e and 11f. Ideally the boundary is defined by a marked change in mineralogy which includes biotite, the presence of cordierite, as well as an abrupt change towards a coarser grain size in the leucocratic segregation. This is readily observed in thin sections that were prepared parallel to the lineation. In thin sections where this is not easily visible the absence of cordierite from the leucosomes, apart from that associated with garnet, can be used to distinguish the layers. The leucosome segregations do not show mineral alignment as opposed to the melanosome, which hosts aligned biotite and sillimanite.

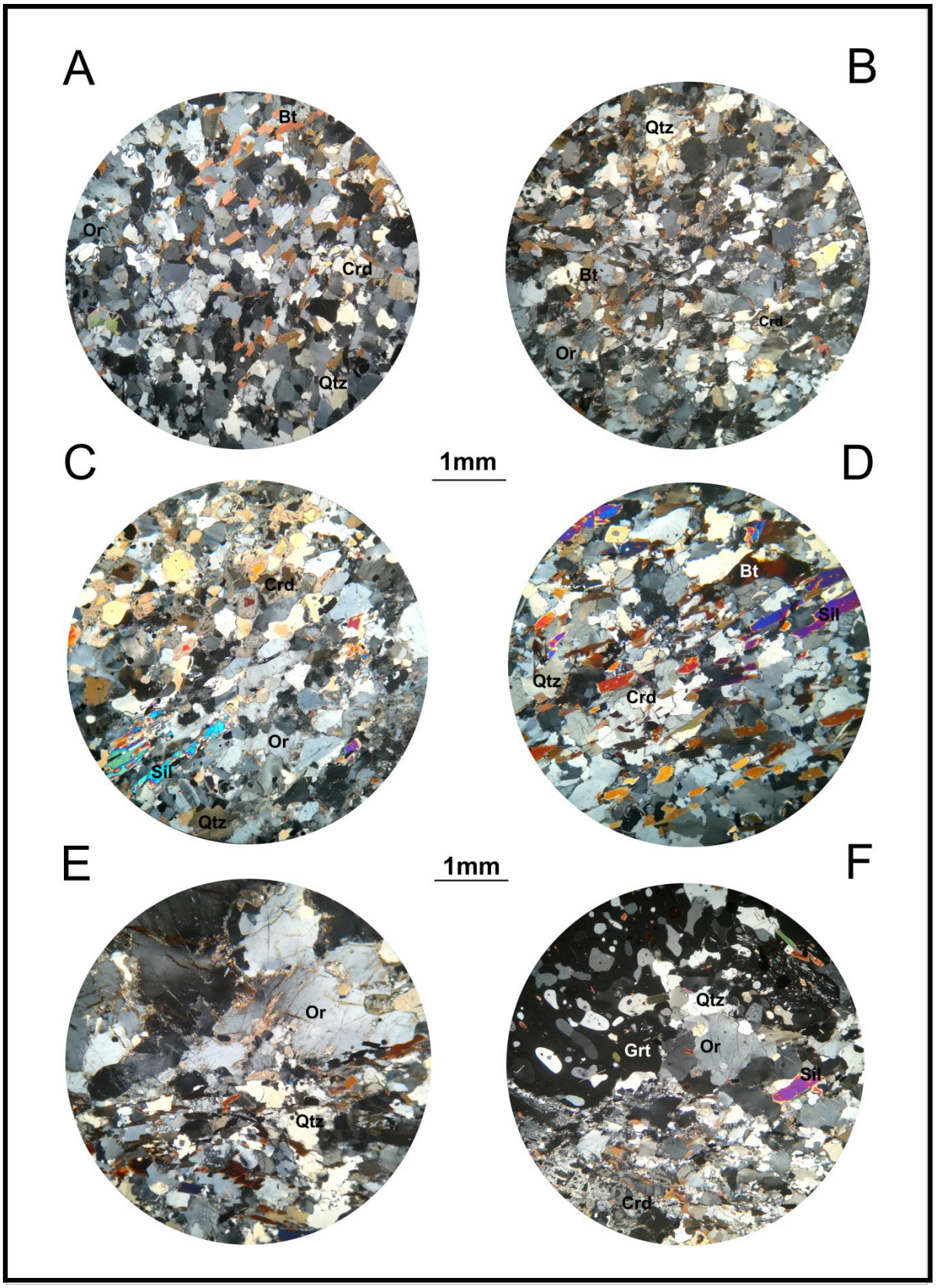

Figure 11: *Photomicrographs displaying melanosomes with and without sillimanite and the contact between the two segregations under crossed polars.. A – B represents melanosomes without sillimanite in the field of view, whilst C – D represent melanosomes with sillimanite in the field of view. E – F illustrates the boundary between the melanosome and leucosomes. The lower parts of these two photomicrographs (E and F) display the melanosomes, whilst the coarser upper part displays the leucosome. A – KL 1b, B – KL 26b, C – KL 6a, D – KL 32a, E – KL 6a, F – KL 13b. Or – Orthoclase, Grt – Garnet, Bt – Biotite, Qtz – Quartz, Crd – Cordierite, Sil – Sillimanite.*

There are various accessory minerals present in these samples, besides opaque minerals. These opaque minerals could include magnetite and ilmenite. Identifiable accessory minerals (Figure 12) include zircon, which is abundant throughout (present in every thin section examined). Rutile, is present in certain samples (Table 1). The spinel group mineral hercynite (Figure 12) is present in minute quantities (typically no more than a few grains) in certain thin sections and occurs as inclusions within garnet, as an overgrowth on cordierite and in association with sillimanite. These minerals surrounding the hercynite have been interpreted by Macey et al. (2011) as high-temperature retrograde coronas. Hercynite – quartz contacts are rarely preserved. Hercynite is absent from the vein samples. Minerals within these samples display a variety of alterations. Evidence of retrograde alteration is exemplified by pinitized cordierite as well as the presence of chlorite and sericite.

Deformation at the thin section scale is apparent in all samples. This is mainly due to the presence of deformed quartz grains. The full spectrum of quartz recrystallization textures is present in the samples. Deformed quartz is also present around garnet grains. This rim of quartz around a garnet is referred to by some authors as a 'moat' (Sawyer, 2008), which separates the garnet from the feldspar. According to Sawyer (2008), this microstructure is typical for biotite dehydration melting. Quartz in the melanosomes tends to have more tabular grain shapes as a result of the preferred orientation of biotite and sillimanite. This is also true for quartz in association with sillimanite in the leucosome. Quartz situated in the leucosomes commonly exhibit lobate grain boundaries and undulose extinction, which, according to Sawyer (2008), is common in leucosomes of regional metamorphic terranes. Sillimanite is aligned in both segregations, but more strongly in the melanosome. Aligned biotite is present in the melanosomes as well. The alignment of sillimanite and biotite gives rise to both nematoblastic as well as lepidoblastic textures. The preferred orientation of sillimanite is representative of the S_2 fabric (Macey et al., 2011).

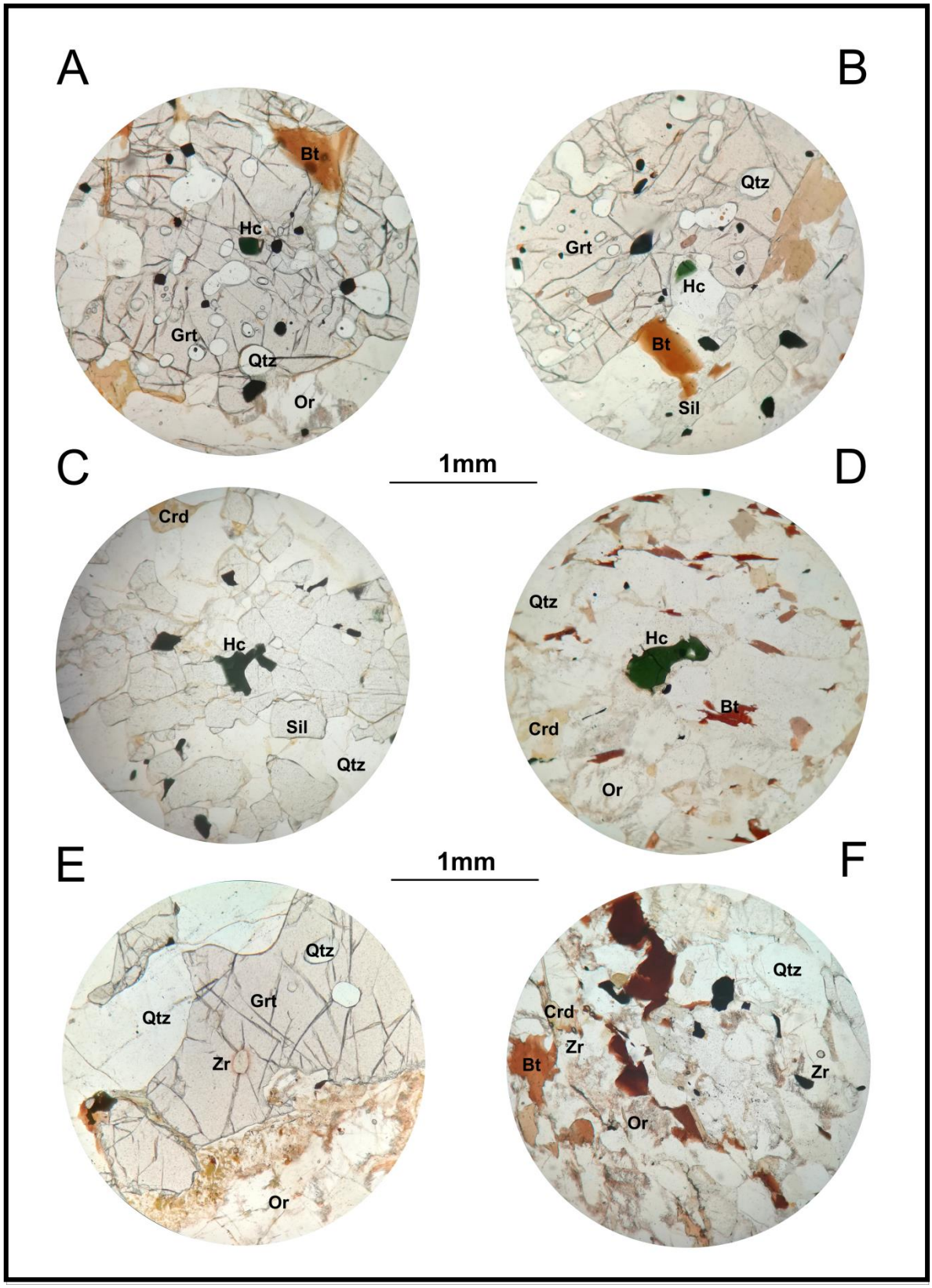

Figure 12: *Photomicrographs showing the various accessory phases in plane-polarized-light. A – D illustrate the occurrences of hercynite in both the leucosome (A and B) and melanosome (C – D). E – F illustrate occurrences of zircon. A – KL 21, B – KL 4a, C – KL 23b, D – KL 26b, E - KL 13a, F – KL 12b. Or – Orthoclase, Grt – Garnet, Bt – Biotite, Qtz – Quartz, Crd – Cordierite, Sil – Sillimanite, Opq – Opaque, Hc – Hercynite, Zr – Zircon.*

Table 1: Mineralogy of the samples with grain size and abundance

Sample	Leucosome			Melanosome			
	Minerals	Grain Size (mm)	Abundance (area%)	Minerals	Grain Size (mm)	Abundance (area%)	Other Features
KL1	Qtz	0.05 – 0.8	32	Or	0.15 – 1	30	
	Or	0.1 – 2.5	30	Qtz	0.05 – 0.8	25	
	Grt	0.5 – 5	20	Crd	0.1 – 0.8	16	
	Sil	0.15 – 1.25	12	Bt	0.05 – 0.5	12	
	Opq	0.05 – 0.15	5	Sil	0.15 – 0.5	10	
				Opq	0.05 – 0.5	5	
				Pl	0.05 – 0.4	2	
KL4	Or	0.05 – 2	34	Or	0.4 – 1	30	-Accessory Rt and Hc -Very large Grt
	Qtz	0.05 – 3	28	Qtz	0.2 – 0.8	28	
	Grt	0.1 – 15	20	Sil	0.2 – 2	15	
	Sil	0.15 – 2	15	Bt	0.2 – 1	12	
	Opq	0.05 – 0.5	3	Crd	0.15 – 0.8	10	
				Opq	0.025 – 0.35	5	
KL5	Qtz	0.15 – 2.5	33	Qtz	0.1 – 1.5	28	- Grt clusters as large as 2cm - Very coarse Sil
	Grt	0.5 – 5	25	Or	0.2 – 1.2	24	
	Pl	0.2 – 1.75	20	Crd	0.25 – 1.35	15	
	Or	0.2 – 2	20	Bt	0.1 – 1.5	15	
	Opq	0.05 – 0.25	2	Sil	0.1 -2.5	13	
				Opq	0.05 – 0.6	5	
KL6	Or	0.2 – 2.7	38	Qtz	0.1 – 0.4	28	- Grt aggregates up to 7mm - Very coarse Sillimanite (up to 4mm) - Accessory Hc
	Qtz	0.1 – 1.8	28	Or	0.15 – 1	22	
	Grt	0.4 – 5.2	26	Bt	0.05 – 1.75	20	
	Sil	0.15 – 2.5	6	Sil	0.1 – 0.4	13	
	Opq	0.025 – 0.5	2	Crd	0.2 – 0.8	11	
				Pl	0.15 – 0.6	3	
				Opq	0.025 – 0.4	3	
KL7	Grt	0.2 – 7.5	33	Qtz	0.05 – 1.5	30	- Grt clusters as large as 1.5cm - Very coarse Sil
	Or	0.2 – 2	32	Sil	0.1 – 5	20	
	Qtz	0.1 – 2	23	Crd	0.15 – 1	17	
	Pl	0.2 – 0.6	11	Bt	0.1 – 1.25	13	
	Opq	3	3	Or	0.2 -1.2	11	
				Opq	0.05 – 0.8	5	
				Pl	0.2 – 1	4	
KL9	Or	0.2 – 2.2	45	Qtz	0.1 – 2	30	- Grt clusters as large as 1.5cm
	Qtz	0.1 – 2.2	35	Crd	0.2 – 1.25	20	
	Grt	0.55 – 5	14	Bt	0.05 – 1.5	16	
	Sil	0.1 – 1.5	4	Sil	0.15 – 3	14	
	Opq	0.05 – 0.5	2	Or	0.2 – 1	13	
				Opq	0.05 – 0.75	5	
				Pl	0.2 – 0.5	2	
KL11	Or	0.1 – 2.7	45	Qtz	0.05 – 1.1	30	-Accessory Hc
	Qtz	0.05 – 2.2	35	Or	0.15 – 1	26	
	Grt	0.4 – 7	18	Crd	0.15 – 0.4	16	
	Opq	0.025 – 0.7	2	Bt	0.05 – 0.3	14	
				Sil	0.1 – 2.2	10	
				Opq	0.05 – 0.25	4	
KL12	Or	0.2 – 1.5	42	Qtz	0.1 – 0.3	28	-Accessory Hc
	Qtz	0.1 - 1	28	Sil	0.15 – 2	26	
	Grt	0.3 – 3	26	Or	0.1 - 1	22	
	Opq	0.05 – 1.1	4	Crd	0.05 – 0.8	13	
				Bt	0.05 – 1.2	8	
				Opq	0.025 – 1.1	3	

Grt – Garnet, Qtz – Quartz, Kfs – K-feldspar, Sil – Sillimanite, Bt – Biotite, Pl – Plagioclase, Crd – Cordierite, Opq – Opaque Minerals, Zr – Zircon, Rt - Rutile, Hc.

Table 1: ***Continued***

Sample	Leucosome			Melanosome			
	Minerals	Grain Size (mm)	Abundance (area%)	Minerals	Grain Size (mm)	Abundance (area%)	Other Features
KL13	Or	0.25 – 1.5	45	Or	0.2 – 1	30	-Accessory Hc
	Qtz	0.1 – 1	35	Qtz	0.1 – 1	26	
	Sil	0.1 – 0.4	10	Crd	0.25 – 1.25	22	
	Grt	1 – 5.5	8	Bt	0.05 – 0.5	10	
	Opq	0.05 – 0.5	2	Sil	0.1 – 1.25	10	
				Opq	0.05 – 0.5	2	
Vein-type leucosome	Or	0.2 - 6	50	- Relatively opaque free, opaque minerals limited to Grt			
	Qtz	0.1 – 6.25	37	- Accessory Rt			
	Grt	1.25 - 6	8	- Accessory Zr			
	Sil	0.15 – 0.8	5				
KL20	Or	0.1 – 2.5	40	Qtz	0.1 - 2	30	- Very coarse Sil
	Qtz	0.1 – 2	25	Crd	0.2 – 1.25	22	
	Grt	0.5 – 5	20	Sil	0.2 – 0.65	20	
	Sil	0.1 – 5	10	Or	0.2 – 1	13	
	Opq	0.05 – 0.3	5	Bt	0.1 – 1.2	10	
				Opq	0.05 - 1	5	
KL 21	Or	0.8 – 2.5	43	Qtz	0.2 – 1.25	30	-Accessory Rt and Hc -Large sillimanite grains (up to 5mm)
	Qtz	0.1 – 2.5	32	Or	0.4 – 1.25	22	
	Grt	0.8 – 5.5	20	Crd	0.3 – 1.1	20	
	Sil	0.5 - 5	12	Sil	0.15 – 3	18	
	Opq	0.05 – 0.6	2	Bt	0.15 – 1.3	8	
				Opq	0.05 – 0.25	2	
KL23	Qtz	0.1 – 1.5	34	Qtz	0.1 – 1.75	29	-Accessory Hc
	Or	0.25 – 1.6	28	Or	0.4 – 1.6	24	
	Sil	0.1 – 3	20	Sil	0.1 – 1.5	20	
	Grt	0.5 – 3.75	15	Crd	0.1 – 2	17	
	Opq	0.05 – 0.5	3	Bt	0.05 - 0.8	9	
				Opq	0.05 – 0.5	2	
KL25	Or	0.25 – 5.5	36	Qtz	0.25 – 1.5	30	- Grt clusters as large as 1cm
	Grt	0.4 - 5	25	Crd	0.2 – 1.5	20	
	Qtz	0.2 – 4.75	20	Or	0.2 – 1	17	
	Sil	0.1 – 5	6	Sil	0.2 – 5.2	15	
	Opq	0.05 – 0.75	3	Pl	0.2 – 0.75	8	
				Bt	0.1 – 1	7	
				Opq	0.05 - 1	3	
KL26	Or	0.25 – 2.5	40	Qtz	0.1 – 1.25	29	- Very coarse Sil -Accessory Hc
	Qtz	0.1 – 2.5	27	Or	0.05 – 1	23	
	Grt	0.4 – 7.5	25	Crd	0.25 – 1	20	
	Sil	0.1 – 2.5	5	Sil	0.1 – 5	13	
	Opq	0.05 – 0.25	3	Bt	0.05 –1	11	
				Opq	0.05 – 0.6	3	
KL 32	Or	0.5 - 1	38	Crd	0.2 – 1.25	35	-Accessory Hc
	Qtz	0.1 – 0.5	34	Qtz	0.05 – 0.5	30	
	Grt	1.5 – 3.5	25	Or	0.5 - 1	20	
	Opq	0.05 – 0.25	3	Opq	0.05 – 0.25	8	
				Bt	0.25 – 0.5	5	
				Sil	0.1 – 0.5	2	
Vein-type leucosome	Or	0.5 – 5	55	- Very coarse grained			
	Qtz	0.25 – 5.5	45	- Opaque free			

Grt – Garnet, Qtz – Quartz, Kfs – K-feldspar, Sil – Sillimanite, Bt – Biotite, Pl – Plagioclase, Crd – Cordierite, Opq – Opaque Minerals, Zr – Zircon, Rt - Rutile, Hc.

5. Geochemstry: Analytical data and their evaluation

Nine samples were selected for geochemical analysis. Of these nine samples, six showed relatively well-defined leucosome and melanosome domains; two are migmatite samples in which the leucosomes are so intimately interlayered with the melanosomes that a physical separation for bulk analyses is not possible (KL20 and KL25). The last sample is a vein-type leucosome (KL13) that cross-cuts the existing S-L structures which was selected for comparison to the fabric-parallel leucosomes. Samples KL2, KL5A, KL6, KL7, KL9 and KL26 were prepared to study the bulk-chemical relationships between the magmatic and residual fractions which constitute these migmatites.

The geochemical analyses of these migmatites will aid in understanding the processes of anatexis and thus aid in answering the questions: are these migmatites a product of in-situ anatexis, with the leucosome not having migrated from its site of formation, and thus still spatially associated with its melt residuum, the two combining to form the original bulk rock before anatexis? Is there a close relationship preserved between leucosome and melanosome, but modified to some extent through partial melt loss? Or was melt externally derived and injected into an unrelated host rock?

5.1 General geochemical characteristics: Major elements

The major-element geochemical data of the bulk migmatite samples (KL2, KL5A, KL6 etc.) and the leucosome (L) and melanosome (M) fractions are presented in Table 2, which shows that SiO_2 is the most abundant oxide across the sample set, followed by Al_2O_3, Fe_2O_3, K_2O, MgO, Na_2O, CaO, TiO_2, MnO and P_2O_5 in descending order of abundance (Table 2). Using bulk migmatite geochemical data this section aims to determine possible protoliths of the samples collected for this study. The bulk geochemistry listed in Table 2 points to a chemical system dominated by K_2O (Na_2O) – FeO - MgO – Al_2O_3 – SiO_2 – H_2O (K(Na)FMASH) which commonly characterizes metapelites.

5.1.1 Bulk migmatites and melanosomes

Table 3 lists the composition of the bulk migmatite samples of this study to compare it with average pelitic compositions from studies carried out by various authors. This includes the North American Shale Composite (NASC) after Gromet et al. (1984), Post-Archean Australian Shale after Taylor and McLennan (1985), the average of ~100 shale and slate analyses (Ague, 1991), the average of ~150 amphibolite-facies felsic pelitic rocks (Ague 1991), the Average Canadian Proterozoic Shale (Cameron and Garrels, 1980) and the Average Russian Proterozoic Shale (Ronov and Migdisov, 1971).

Table 1: Major element geochemistry of bulk migmatite and segregations (wt. %), *L – Leucosome, M – Melanosome.*

	KL2	KL2 L	KL2 M	KL5A	KL5A L	KL5A M	KL6	KL6 L	KL6 M	KL7	KL7 L	KL7 M
SiO_2	67.78	67.11	69.75	67.76	66.26	69.07	67.90	67.62	69.33	66.91	66.43	68.95
TiO_2	0.89	0.72	1.02	0.87	0.65	1.00	0.88	0.68	1.01	0.89	0.71	1.02
Al_2O_3	16.60	15.56	17.63	16.66	15.64	17.46	17.22	16.25	18.34	17.29	15.84	17.72
Fe_2O_3(t)	5.97	7.94	3.85	6.66	9.36	3.69	6.23	8.48	3.89	7.02	9.09	3.96
MgO	2.00	1.95	2.38	2.25	2.32	2.44	2.12	2.10	2.43	2.22	2.29	2.32
MnO	0.10	0.15	0.03	0.08	0.13	0.01	0.07	0.12	0.02	0.11	0.15	0.02
CaO	0.81	0.73	0.61	0.92	0.68	0.84	0.74	0.62	0.65	0.96	0.85	1.03
Na_2O	1.40	1.30	1.10	1.18	0.93	1.21	0.93	0.79	0.83	1.25	1.16	1.40
K_2O	4.39	5.02	2.96	3.57	4.60	3.48	3.56	3.81	2.86	3.35	4.08	2.90
P_2O_5	0.06	0.08	0.04	0.06	0.08	0.05	0.07	0.08	0.04	0.07	0.09	0.05
L.O.I.	0.78	0.17	1.18	0.61	0	1.30	0.66	-0.09	1.25	0.45	-0.04	1.19
Sum	100.78	100.73	100.55	100.62	100.65	100.55	100.38	100.46	100.65	100.52	100.65	100.56

Table 2: Continued

	KL9	KL9 L	KL9 M	KL13	KL20	KL25	KL26	KL26 L	KL26 M
SiO_2	67.72	65.77	68.61	73.73	64.90	64.49	66.07	66.48	67.16
TiO_2	0.87	0.67	0.98	0.20	0.80	0.82	0.84	0.69	1.00
Al_2O_3	17.10	15.84	17.78	13.61	19.82	19.72	17.67	16.51	18.25
Fe_2O_3(t)	6.93	9.99	4.09	4.48	7.79	7.86	7.38	9.08	4.03
MnO	0.08	0.13	0.02	0.09	0.11	0.11	0.10	0.14	0.02
MgO	2.29	2.46	2.61	1.04	1.79	1.84	2.21	2.19	2.64
CaO	0.73	0.71	0.76	0.36	1.06	0.85	0.69	0.62	0.78
Na_2O	0.85	0.78	0.97	1.13	0.88	0.81	0.85	0.68	1.04
K_2O	3.21	4.10	3.17	5.71	3.26	3.63	3.99	4.15	3.82
P_2O_5	0.06	0.09	0.05	0.06	0.05	0.06	0.06	0.07	0.04
L.O.I.	0.73	-0.12	1.57	0.24	0.37	0.36	0.73	-0.09	1.59
Sum	100.57	100.42	100.61	100.65	100.83	100.55	100.59	100.52	100.37

Table 2: Bulk migmatite composition of studied samples in comparison to published averages of pelitic rocks.

	SiO_2	TiO_2	Al_2O_3	FeO	MnO	MgO	CaO	Na_2O	K_2O	P_2O_5
KL2	67.78	0.89	16.60	6.63	0.10	2.00	0.81	1.40	4.39	0.06
KL5A	67.76	0.87	16.66	7.40	0.08	2.25	0.92	1.18	3.57	0.06
KL6	67.90	0.88	17.22	6.92	0.07	2.12	0.74	0.93	3.56	0.07
KL7	66.91	0.89	17.29	7.80	0.11	2.22	0.96	1.25	3.35	0.07
KL9	67.72	0.87	17.10	7.70	0.08	2.29	0.73	0.85	3.21	0.06
KL20	64.90	0.80	19.82	8.66	0.11	1.79	1.06	0.88	3.26	0.05
KL25	64.49	0.82	19.72	8.73	0.11	1.84	0.85	0.81	3.63	0.06
KL26	66.07	0.84	17.67	8.20	0.10	2.21	0.69	0.85	3.99	0.06
1	64.70	0.80	17.00	5.69	0.25	2.82	3.50	1.13	3.96	0.15
2	64.00	0.81	18.10	7.03	0.10	2.85	1.54	1.64	3.86	0.15
3	56.30	1.05	20.20	8.38	0.18	3.23	1.59	1.86	4.15	-
4	69.64	1.02	18.08	3.57	0.02	2.50	0.79	1.10	3.24	0.05
5	64.17	1.02	19.31	6.64	0.11	2.25	1.33	1.23	3.78	0.16
6	66.90	0.78	16.67	5.87	0.06	2.59	0.53	1.50	4.97	0.14
7	63.04	0.94	18.63	7.66	0.12	2.60	1.31	1.02	4.57	0.10

1: North American Shale Composite (Gromet et al., 1984), **2**: Average of ~ 100 shale and slate analysis, Ague (1991). **3**: Average of ~ 150 amphibolite-facies felsic pelitic rocks, Ague (1991). **4**: Average of melanosomes (this study). **5**: Post-Archean Australian Shale (Taylor and McLennan, 1985). **6**: Average Canadian Proterozoic Shale (Cameron and Garrels, 1980). **7**: Average Russian Proterozoic Shale (Ronov and Migdisov, 1971).

The geochemical data listed in Table 3 are graphically presented in ternary diagrams to provide a clearer understanding of the collective characteristics of the dataset (Figure 13). This includes ternary Al_2O_3 – CaO – K_2O, Al_2O_3 – FeO – MgO and Al_2O_3 – FeO+MgO – K_2O ternary diagrams. These diagrams are used to compare the bulk migmatite sample (and melanosomes) of this study to various references of pelitic composition. The majority of the literature reference data forms a relatively tight cluster. In the Al_2O_3-CaO-K_2O ternary diagram, NASC plots as an outlier, due to the significantly larger CaO content compared to the other datasets. This shift away from the other compositions reflects the relatively high Ca-carbonate levels in the NASC shale data set. It must be emphasized that the literature data points are averages, and that the compositional spread of the different data sets would show an extensive overlap between them. As presented in Figure 13 and Table 3, the bulk migmatite data compares well to the averages of the literature data, plotting within the cluster of reference data.

The melanosomes, unlike the bulk migmatite sample, consistently plot away from the cluster of reference data, clearly displaying much less of an affinity to metapelites.

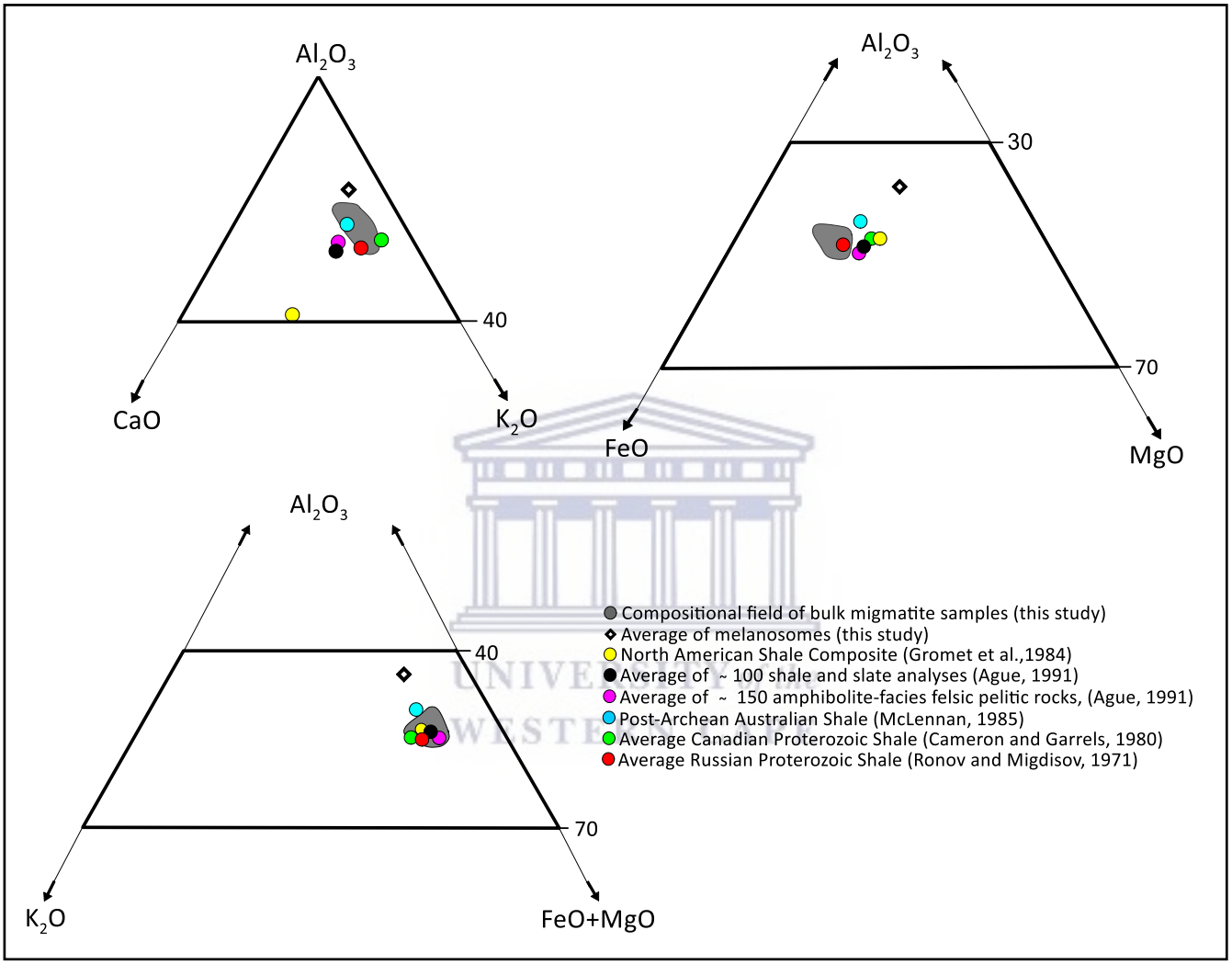

Figure 13: ***A*** *- Al_2O_3 - CaO - K_2O,* ***B*** *- Al_2O_3 - FeO – MgO,* ***C****- Al_2O_3 - K_2O-FeO+MgO ternary diagrams comparing the compositional spread of the Kliprand (KL) bulk migmatite samples of this study with the literature data of pelitic and metapelitic rocks. The average of melanosome compositions of the KL samples are also shown for comparison. FeO has been recalculated from the Fe_2O_3(t) values.*

5.1.2 Leucosomes

The leucosomes, representative of the melt fraction, are plotted on various classification diagrams (Figure 14) in order to assess their geochemical affinities. The leucosomes are distinctly peraluminous (Figure 14A), reflecting their metapelitic protoliths, and exhibit an alkali-calcic to calc-alkalic composition (Figure 14B). The leucosomes plot along the border of the ferroan-magnesian divide and are slightly more magnesian (Figure 14C). They exhibit compositions largely similar to a syeno-granite with one sample showing a composition similar to that of a monzo-granite when plotted on a QAP diagram (Figure 14D). The vein-type leucosome displayssimilar geochemical affinities as the fabric-parallel leucosomes, but plots away from the other leucosome group in figures 14B and C

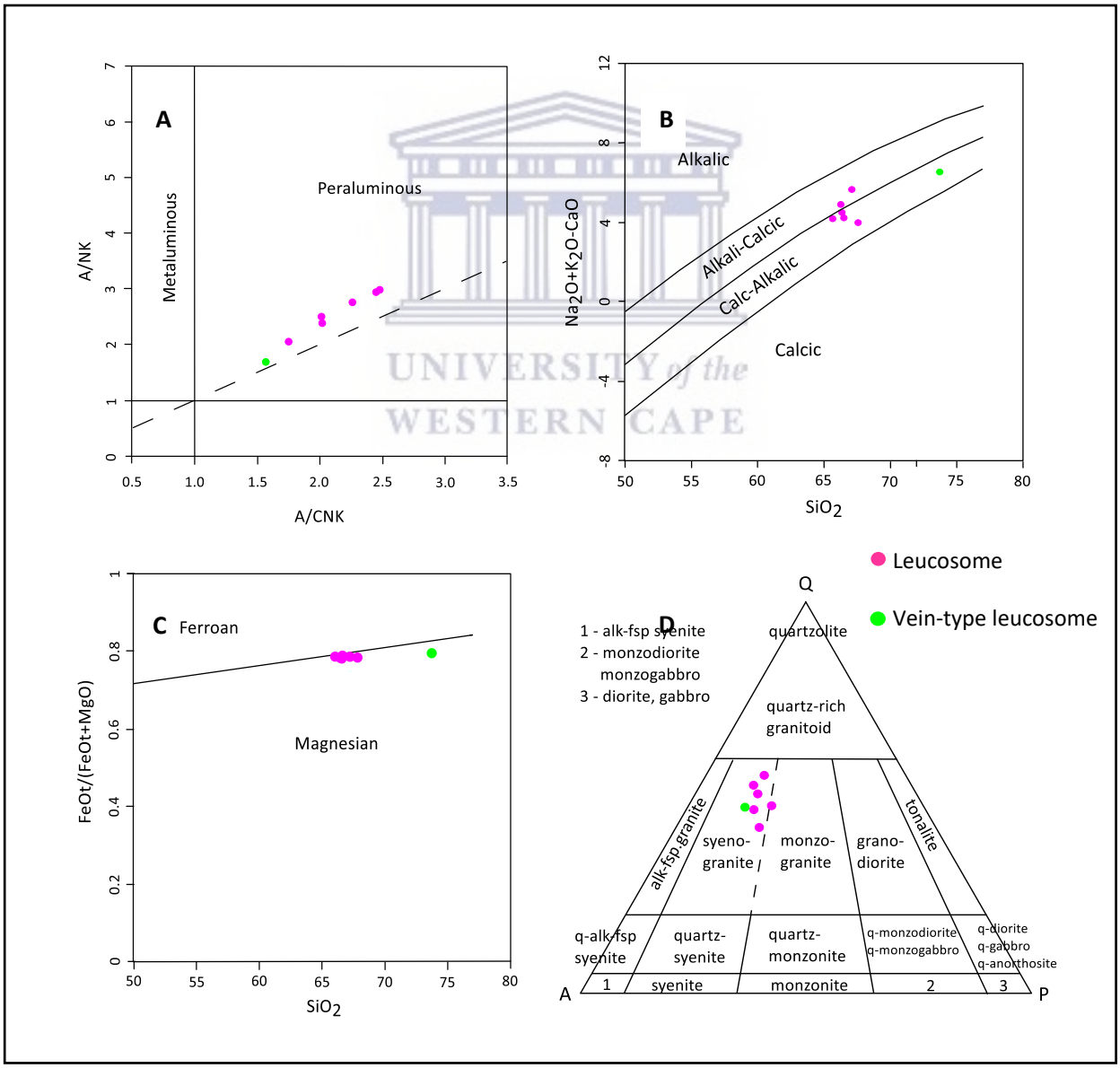

Figure 14: A - *A/CNK vs A/NK after Shand (1943).* B – *Na_2O+K_2O-CaO (wt.%) vs SiO_2 (%) after Frost et al. (2001).* C – *FeOt/(FeOt+MgO) (wt.%) vs SiO_2 (wt.%) after Frost and Frost (2008).* D - *QAP classification diagram after Streckeisen (1974).*

Further comparison between the samples of this present study and reference data is illustrated in Figure 15A (after Sawyer, 2008). Herein the dashed-line polygon represents experimental quenched partial melts of pelitic protoliths formed from dehydration melting mechanisms. It encompasses a pressure range from <3.5 kbar to >20 kbar as well as melts formed below 925°C and those formed above 925°C. The leucosomes of this study plot within this field which further emphasizes the pelitic affinity of the samples. This is in concurrence with Figure 15B (after Laurent et al., 2014) which implies that the source of the melt fraction is metasedimentary. Figure 16, after Altherr et al. (2000), shows the leucosomes plotting close to the field of partial melts that originated from a metapelitic source. The inset enlargement shows the effect which the large proportion of garnet has on the leucosome composition, essentially drawing the compositions towards it. The inset also displays the compositional trend of the leucosomes if garnet were removed, as indicated by the arrow, which is toward the liquid melt phase. The effect which garnet has on the leucosome is further emphasized in Figure 17 where the leucosomes (representative of the melt fraction) are drawn towards more typical residual compositions. The vein-type leucosome has a metapelitic source (Figure 16) and can be seen to possess a composition close to that of an anatectic melt (Figure 17). Table 3, as well as Figures 13, 15A, 15B and 16 all concur with an initial metapelitic protolith for the samples of this study.

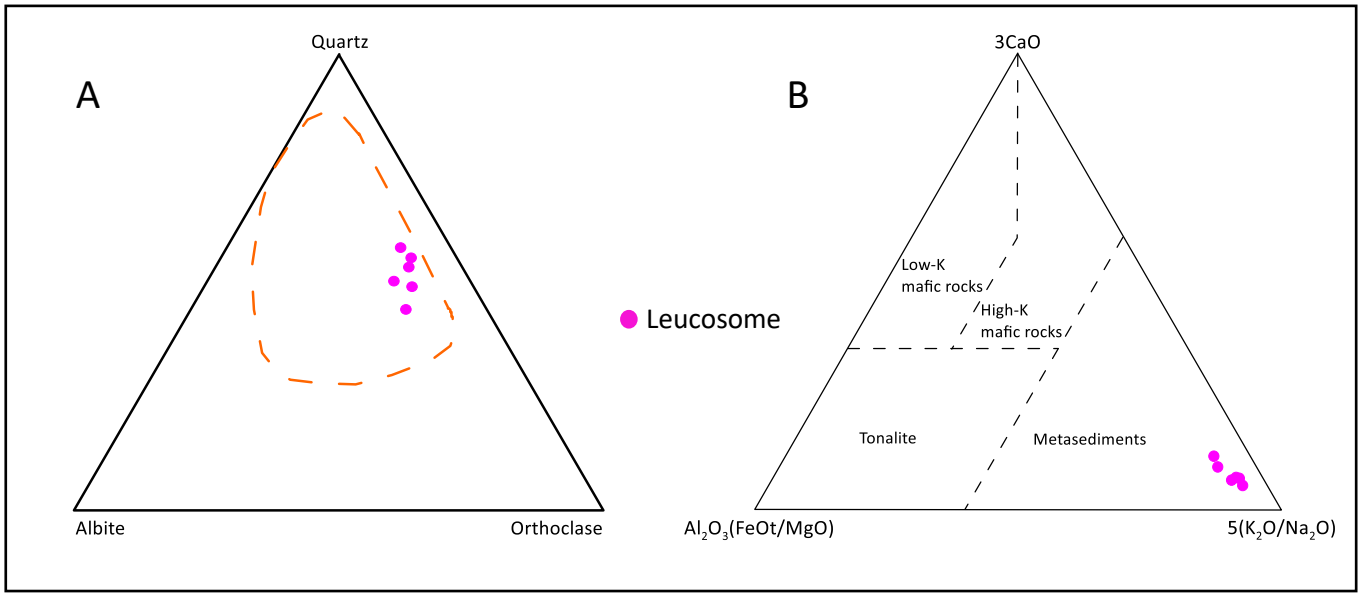

Figure 15: A – *Qtz-Ab-Or diagram after Sawyer (2008).* **B** – *3CaO vs Al_2O_3(FeOt/MgO) vs 5(K_2O/Na_2O) after Laurent et al. (2014).*

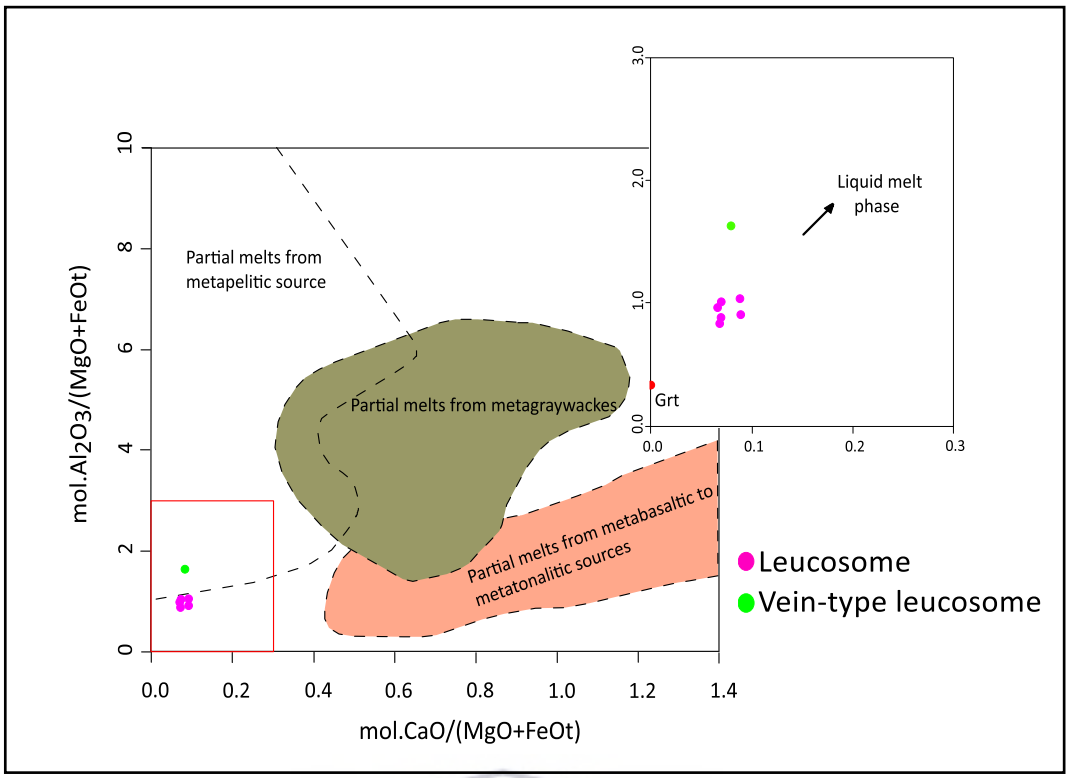

Figure 16: mol. *Al_2O_3/(MgO+FeOt) vs mol. CaO/(MgO+FeOt) fields after Altherr et al. (2000). The inset in the top left corner represents a magnified view of the area demarcated by the red rectangle.*

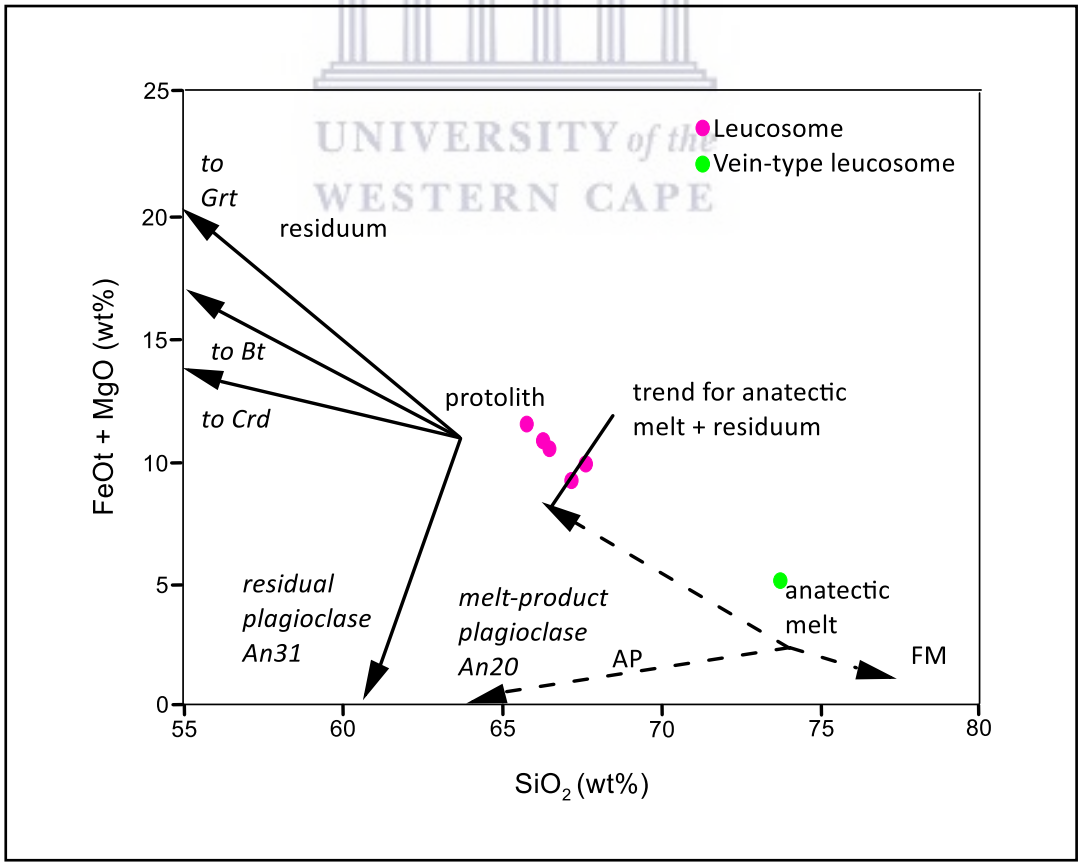

Figure 17: *FeOt + MgO vs SiO_2, trends are representative of those for pelitic migmatites of the Quetico Subprovince (Sawyer (2008). AP – Accumulation of plagioclase, FM – Fractionated melt.*

5.2 General geochemical characteristics: Trace elements

Trace elements are presented in Tables 4 (trace elements other than REE) and 5 (rare earth elements (REE)). Diagnostic tests performed after LA-ICPMS analysis of the trace data revealed the milling process, specifically, the length of milling times and the type of milling bowl used, resulted in skewed values for V, Cr, Ni, Cu and Mo. The values for these elements are reported here in Table 4. The graphical effect of the length of milling times on these element abundances are displayed in Appendices B and C. These trace elements affected by contamination through milling are, however, not critical for this study and will not be considered further in the discussions.

The trace element composition of the bulk migmatite samples are compared to published averages of pelitic rocks (Table 6) in order to assess any similarities and ultimately complement the major element data in defining the protolith of the bulk migmatite samples of this study. Trace elements are discussed in greater detail along with graphical analyses later in the chapter.

Table 3: Trace element geochemistry of bulk rocks and segregations (ppm), *L – Leucosome, M – Melanosome.*

	KL2	KL2 L	KL2 M	KL5A	KL5A L	KL5A M	KL6	KL6 L	KL6 M	KL7	KL7 L	KL7 M
Sc	14.9	24.4	3.8	14.4	27.8	2.3	14.8	26.5	3.2	17.38	28.8	3
V	111	97.1	126	110.8	78.2	135	114	88.7	137	113	85.4	142
Cr	294	289	303	294	281	293	338	292	297	300	291	335
Co	14.2	16.5	12.9	15.3	17.3	14.2	14.2	15.0	14.5	14.9	16.2	14.1
Ni	25.3	17.5	36.5	32.6	16.2	59.0	33.4	16.4	57.0	29.5	16.3	55.6
Cu	6.15	8.9	5.7	5.8	9.1	7.5	5.3	5.4	5.1	5.4	6.0	5.9
Zn	91.8	72.5	115	104	88.9	141	96.9	81.8	125	101	82.5	128
Rb	151.3	161	118	145	158	181	152	133	161.2	141	145	166
Ba	869	1018	574	861	1137	820	836	922	647.8	763	919	644
Sr	79.3	83	57.4	74.2	85.4	71.5	79.8	83.6	63.7	68.5	74.1	64.7
Cs	6.9	3.7	11.9	9.3	4.6	17.6	10.6	4.7	18.1	9.9	4.8	19.1
Zr	216	189	241	208	168	237	196	167	224	209	171	232
Nb	14.4	11.8	16.3	14.1	11.7	15.1	14.4	11.9	15.6	14.5	11.8	15.3
Y	40.5	68.5	7.6	35.6	75.1	2.8	38.2	70.8	5.3	42.6	75.6	5.7
Ta	1	0.84	1.1	0.96	0.89	0.93	0.98	0.89	0.97	0.99	0.88	0.96
Hf	6.3	5.4	7.2	6.1	5.0	7.0	5.7	4.9	6.8	6.0	5.0	7.0
Pb	21.4	24.6	14.0	14.9	20.3	12.6	14.2	17.3	10.1	14.2	17.7	11.1
Th	14.1	21.1	13.3	13.1	23.5	7.2	14.0	22.0	12.0	14.1	18.9	10.4
U	1.77	2.5	1.8	1.7	2.6	1.1	1.8	2.7	1.6	2.0	2.7	1.6
Mo	12.3	13.6	12.5	13.4	13.1	12.8	15.1	14.2	12.2	13.4	13.6	14.4

Table 4: Continued

	KL9	KL9 L	KL9 M	KL13	KL20	KL25	KL26	KL26 L	KL26 M
Sc	15.1	32.3	2.5	18.2	16.3	15.9	16.4	24.7	2.4
V	115	89.3	129	61.9	118	120	120	104	129
Cr	317	284	330	340	295	331	347	300	317
Co	15.4	17.9	14.4	8.4	16.9	17.0	15.2	16.4	14.0
Ni	29.9	16.1	49.6	10.2	28.0	33.9	19.9	11.8	35.3
Cu	9.6	6.8	6.3	10.1	9.0	12.4	8.8	5.8	6.4
Zn	101	85.9	135	42.4	99.6	105	109	83.9	153
Rb	116	123	145	202	124	138	134	124	159
Ba	765	945	736	1280	650	679	941	959	855
Sr	71.0	81.7	71.3	112	108	106	79.9	78.4	81.3
Cs	7.3	3.4	13.9	5.9	3.1	3.6	4.9	2.4	10.1
Zr	188	161	218	389	206	211	177	161	209
Nb	14.0	11.5	15.3	3.4	14.9	15.2	14.1	11.5	15.6
Y	36.2	81.5	4	54.5	46.7	45.4	38.8	63.1	2.7
Ta	0.96	0.86	0.95	0.27	1	1	0.97	0.88	0.97
Hf	5.5	4.8	6.5	13.1	6.3	6.4	5.2	4.8	6.2
Pb	10.1	13.9	9.0	24.2	13.0	13.9	16.9	18.5	15.1
Th	13.7	20.7	9.6	21.2	17.5	17.6	14.9	24.0	6.3
U	1.8	2.6	1.2	3.4	1.8	2.0	1.7	2.7	0.9
Mo	14.3	13.2	14.6	24.6	13.4	15.9	15.9	13.3	14.0

Table 4: Rare earth element geochemistry of bulk rock and segregations*, L -Leucosome, M – Melanosome.*

Rare Earth Elements (ppm)

	KL2	KL2 L	KL2 M	KL5A	KL5A L	KL5A M	KL6	KL6 L	KL6 M	KL7	KL7 L	KL7 M
La	42.4	59.4	37.7	37.1	58.3	23.8	40.8	60.1	34.1	40.5	52.17	32.2
Ce	88.8	127	80.0	75.0	122	45.9	83.8	127	70.6	83.6	111	66.3
Pr	10.6	15.6	9.7	9.0	14.8	5.3	10.0	15.3	8.4	9.9	13.6	7.8
Sm	8.1	12.9	6.9	6.7	11.6	3.5	7.9	12.6	6.0	8.0	11.5	5.6
Eu	1.4	1.6	0.96	1.4	1.8	1.2	1.5	1.7	1.0	1.4	1.7	1.1
Gd	7.7	12.1	4.1	6.3	11.1	1.8	7.1	12.1	3.6	7.4	11.5	3.3
Tb	1.2	2.0	0.38	1.0	1.8	0.16	1.1	2.0	0.31	1.2	1.9	0.3
Dy	7.4	12.6	1.8	6.6	12.6	0.67	6.9	13.0	1.3	7.7	13.0	1.4
Ho	1.5	2.6	0.3	1.3	2.8	0.1	1.4	2.6	0.19	1.6	2.9	0.21
Er	4.4	7.6	0.8	4.0	9.6	0.27	4.2	8.1	0.54	4.8	9.0	0.53
Tm	0.63	1.1	0.11	0.57	1.5	0.03	0.58	1.1	0.07	0.68	1.3	0.07
Yb	3.9	7.2	0.75	3.7	10.3	0.27	3.9	7.4	0.51	4.5	9.1	0.41
Lu	0.6	1.1	0.12	0.58	1.6	0.04	0.57	1.1	0.09	0.65	1.3	0.07

Table 5: Continued

	KL9	KL9 L	KL9 M	KL13	KL20	KL25	KL26	KL26 L	KL26 M
La	40.9	58.6	28.6	43.1	49.7	52.8	43.9	65.9	24.2
Ce	84.1	123	57.1	88.5	97.0	103	90.6	140.8	45.0
Pr	10.1	15.0	6.8	10.5	11.8	12.5	10.9	17.2	5.2
Sm	8.0	12.5	4.8	7.7	9.2	9.7	8.6	13.6	3.1
Eu	1.3	1.7	1.2	1.8	1.5	1.5	1.3	1.5	1.2
Gd	7.2	11.6	2.7	6.6	8.8	9.0	7.8	11.8	1.6
Tb	1.1	2.0	0.26	1.0	1.4	1.3	1.1	1.8	0.15
Dy	6.9	13.9	1.1	8.0	8.7	8.3	7.4	11.5	0.67
Ho	1.4	3.1	0.14	2.1	1.7	1.7	1.5	2.5	0.1
Er	4	9.9	0.34	8.0	5.2	5.0	4.4	7.6	0.24
Tm	0.57	1.5	0.04	1.4	0.72	0.71	0.64	1.1	0.04
Yb	3.8	10.6	0.3	11.0	4.7	4.7	4.2	8.0	0.24
Lu	0.6	1.5	0.05	1.8	0.7	0.69	0.63	1.2	0.04

Table 5: Trace element composition of the studied samples in comparison to published averages of pelitic rocks.

	Rb	Sr	Ba	Y	Zr	Hf	Nb	Ta	Pb	Th
KL2	151	79.3	869	40.5	216	6.3	14.4	1.0	21.4	14.1
KL5A	145	74.2	861	35.6	208	6.1	14.1	1.0	14.9	13.1
KL6	152	79.8	836	38.2	196	5.7	14.4	1.0	14.2	14.0
KL7	141	68.5	763	42.6	209	6.0	14.5	1.0	14.2	14.1
KL9	116	71.0	765	36.2	188	5.5	14.0	1.0	10.1	13.7
KL20	124	109	650	46.7	206	6.3	14.9	1.0	13.0	17.5
KL25	138	106	679	45.4	211	6.4	14.1	1.0	13.9	17.6
KL26	134	79.9	941	38.8	177	5.2	14.1	0.97	16.9	14.9
1	125	142	636		200	6.3		1.1		12.3
2	129	192	527		165	4.8		0.8		10.3
3	163	63.3	533	23.5	178		8.7		29.8	23.6
4	160	200	650	27.0	210	5.0	19.0		20.0	14.6

1: Average Metamorphosed Shale Composite (Gromet et al., 1984). **2**: North American Shale Composite (Gromet et al., 1984). **3**: Average granulite facies metapelite after Dwivedi et al. (2013). **4**: Post-Archean Australian Shale (Taylor and McLennan, 1985).

Table 6: Continued

	U	La	Ce	Yb	V	Sc	Cr	Ni	Co	Cu
KL2	1.8	42.4	88.8	3.9	111	14.9	294	25.3	14.2	6.2
KL5A	1.7	37.1	75.0	3.7	111	14.4	294	32.6	15.3	5.8
KL6	1.8	40.8	83.8	3.9	114	14.8	338	33.4	14.2	5.3
KL7	2.0	40.5	83.6	4.5	113	17.4	300	29.5	14.9	5.4
KL9	1.8	40.9	84.1	3.8	115	15.1	317	29.9	15.4	9.6
KL20	1.8	49.7	97.0	4.7	118	16.3	295	28.0	16.9	9.0
KL25	2.0	52.8	103	4.7	120	15.9	331	33.9	17.0	12.4
KL26	1.7	43.9	90.6	4.2	120	16.4	347	19.9	15.2	8.8
1	2.7	31.1	66.7	3.1		14.9	125	58.0	25.7	
2	2.5	32.6	72.7	2.8		18.0	417	227	28.2	
3	3.1	67.2	144	1.6	65.3	15.0	91.3	34.2	16.5	97.0
4	3.1	38.0	80.0	2.8	150	16.0	110	55.0	23.0	50.0

Trace elements were plotted on various diagrams in order to assess the provenance of the bulk samples and also compare the bulk samples of this study to data from previous studies. The bulk samples are compared here to the Bushmanland Group (BG) metapelites and metaquartzites as well as the Kamiesberg Group lithologies which include metapelites, semi-pelites, feldspathic quartzites and migmatitic metapelites (from Bailie et al., 2019). Figure 18A is used to determine whether the composition of the bulk samples was influenced by either a more mafic or more felsic provenance. The bulk samples plot between the mafic and felsic trend illustrating equal influence from both. Figure 18A further shows the similarity in composition between the bulk samples and PAAS (Post-Archean Australian Shale) and UCC (Upper Continental Crust). The bulk samples also display similar Th and Sc content as the BG metapelites and the Kamiesberg Group supracrustals. Figure 18B is intended to show the overall provenance type and general composition, which, in the case of the bulk samples, is an intermediate composition with a slightly larger felsic component (than mafic). Compositions of the bulk samples here are also similar to the PAAS and UCC and also similar to the range of the Kamiesberg Group and BG metapelites. Figure 18C shows the bulk samples plotting in the basaltic andesite – andesite provenance field. Interestingly, the bulk samples do not plot within the fields of reference data nor does it plot close to PAAS and UCC positions in this diagram. Even though the bulk samples do not exactly plot within the same fields in Figure 18C as the literature their composition is indeed quite similar.

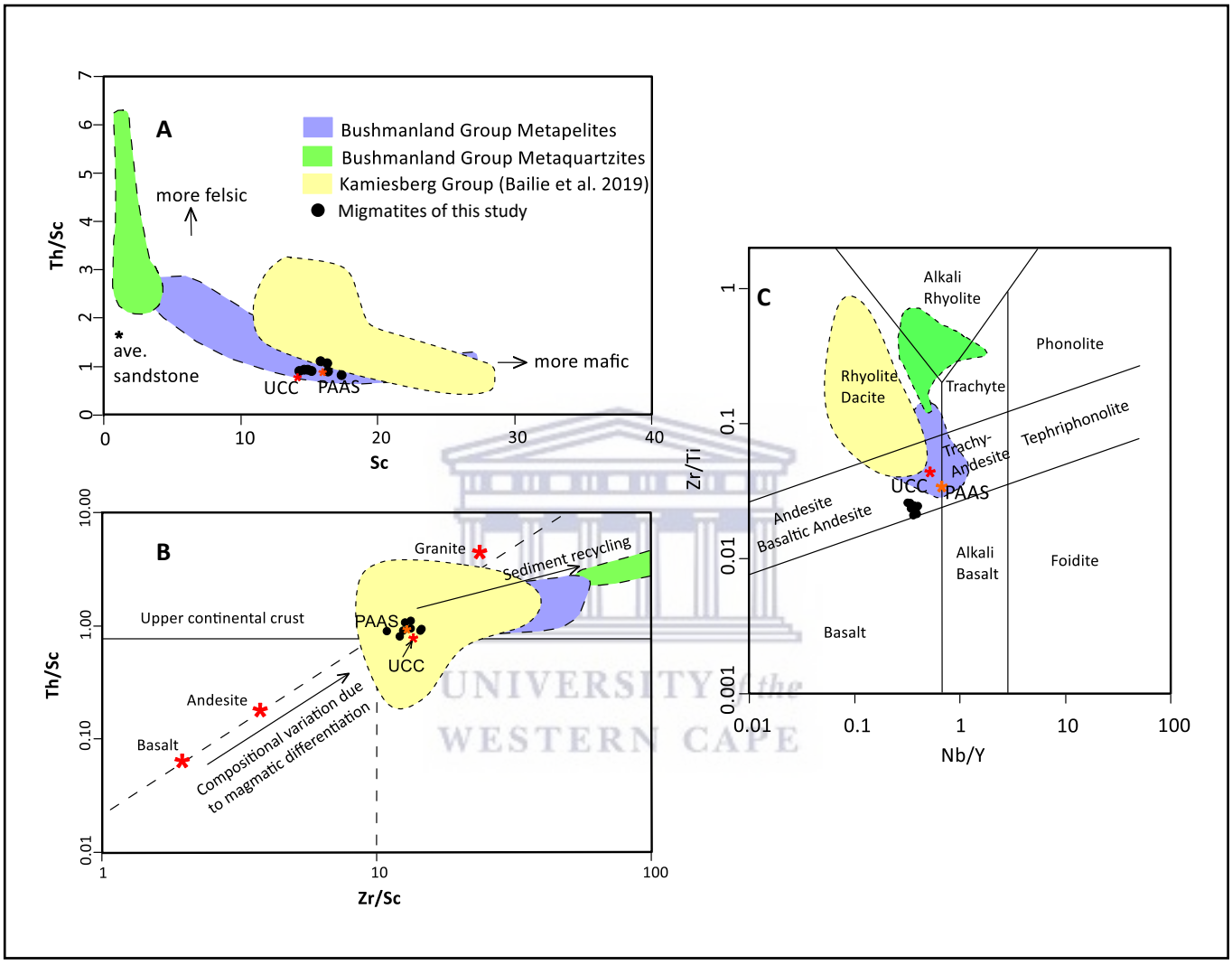

Figure 18: *A – Sc vs. Th/Sc after Taylor and McLennan (1985). B – Zr/Sc vs. Th/Sc plot after McLennan et al. (1976). C – Nb/Y vs. Zr/Ti after Winchester and Floyd (1976). UCC – Upper continental crust, PAAS – Post Archean Australian Shale.*

The trace elements have been normalized to the primitive mantle values of McDonough and Sun (1995). A spider plot of the elements (Figure 19) displays data for the bulk migmatite samples. There is distinct enrichment in the Large Ion Lithophile Elements (LILE) with respect to the High Field Strength Elements (HFSE) displayed here. There are slight depletions in Ba, Zr, Eu and Ti with significant depletions in Nb, Ta and Sr. Slight enrichments are seen in Th and Pb.

The rare earth elements (REE) have been normalized to the primitive mantle values of McDonough and Sun (1995) in Figure 20. The plot represents REE concentrations for the bulk migmatite samples and exhibit enrichment in the LREE with $(La/Lu)_{PM}$ values between 6.54 – 8.02. The bulk migmatite samples display a distinct Eu anomaly with $(Eu/Eu^*)_{PM}$ falling between 0.49 – 0.67. There is little degree of fractionation among the HREE as $(Gd/Lu)_{PM}$ range from 1.36 – 1.67. The LREE, however, exhibit a greater degree of fractionation as $(La/Sm)_{PM}$ range between 3.19 – 3.46.

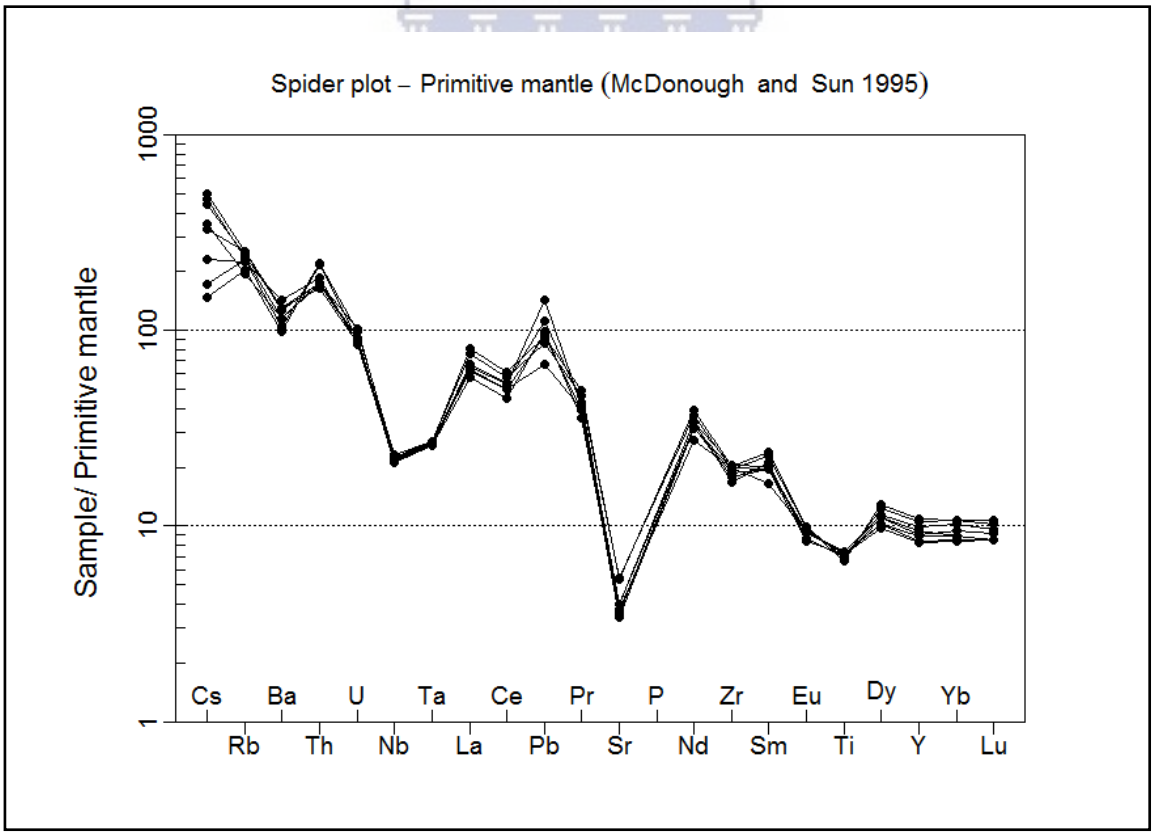

Figure 19: *Primitive mantle-normalized spider diagram (bulk migmatite samples only). Normalized to the values of McDonough and Sun (1995).*

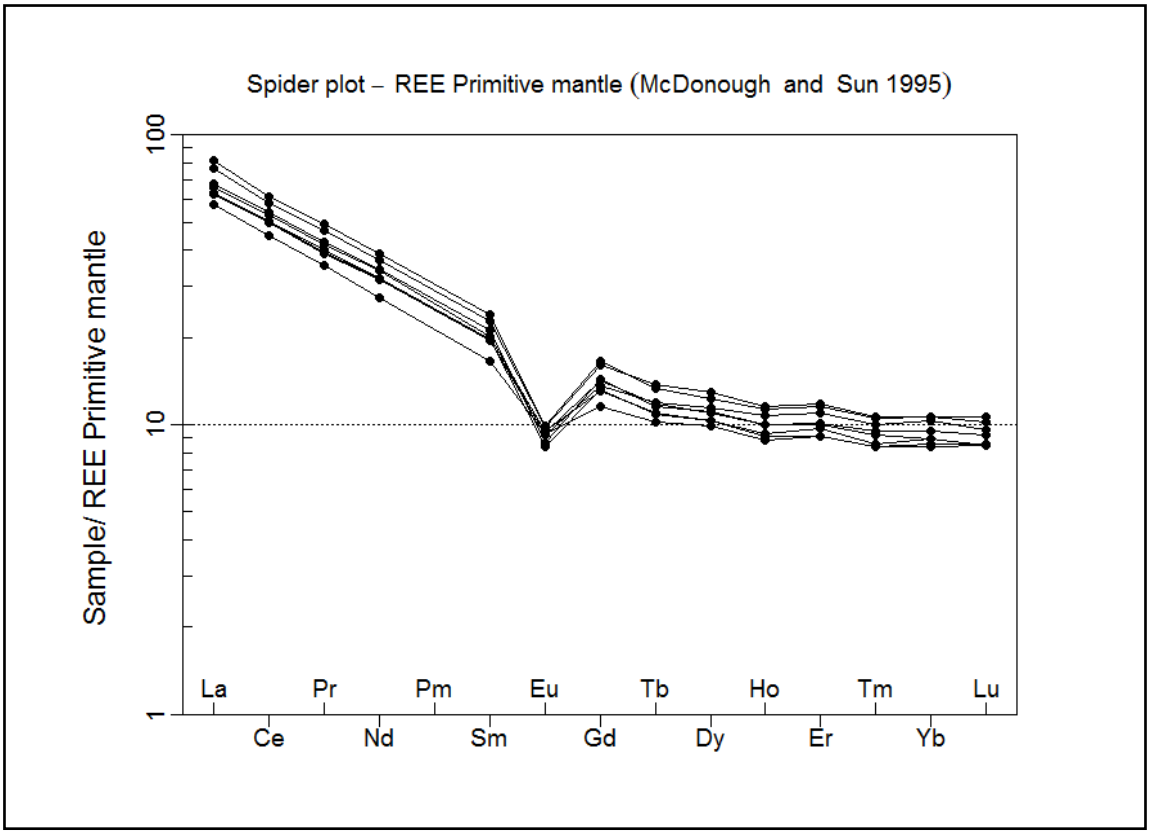

Figure 20: *Primitive mantle-normalized REE diagram (bulk migmatite samples only). Normalized to the values of McDonough and Sun (1995).*

5.3 Geochemical Relations between the leucosome, melanosome, bulk migmatite

5.3.1 Major elements

Variation in major-element abundances between the melanosome (M), leucosome (L) and bulk migmatite datasets are depicted graphically in Figure 21. Ideally, the bulk composition should fall between the leucosome and melanosome compositions that make up a particular sample. Accordingly, the components TiO_2, Al_2O_3, FeO (plotted as Fe_2O_3), MnO and P_2O_5 display a fairly consistent distribution pattern in Figure 21. The SiO_2 and K_2O distributions between bulk sample, melanosome and leucosome are less regular, but it must be noted that, where apparent irregularities occur, the M, L and bulk-rock values are very close to each other, only differing by a small margin of a few percent (relative) to within analytical error between bulk and leucosome or melanosome. MgO, CaO, and Na_2O show a more distinct irregular behaviour in some samples, with the bulk composition not always plotting between melanosome and leucosome.

For MgO, the bulk and leucosome values are almost identical. Hence, the relationship between these is highly sensitive to minor shifts in MgO values (including analytical error). CaO and Na_2O show the most erratic behaviour. Two of the samples show the bulk composition plotting outside of the melanosome-leucosome range, which does not seem logical. There is a distinct similarity between the relative CaO and Na_2O distributions in samples 2 and 6, which points to plagioclase (as the main Ca-Na-bearing phase) being the controlling factor. Thus, the apparent irregular behaviour of specific chemical components in some of the samples can be attributed to primary, pre-anatectic inhomogeneities, which can affect the quality of physical separation of melanosome and leucosome in the preparation lab. Primary compositional inhomogeneities are indeed locally present in some of the samples, in the form of indistinct small-scale banding preserved within the melanocratic part of the samples. The process of physical separation of M and L domains may thus lead to artificially skewed compositional relationships in the diagrams, as with Ca and the alkalis, depending on how well such inhomogeneities are visually identifiable during cutting. As sample parts that could not be clearly assigned to either melanosome or leucosome were discarded, the re-combination of the M and L fractions could therefore deviate marginally from a bulk rock composition.

Furthermore, when separating the melanosome and leucosome physically by cutting, there is inevitably a loss of material. Hence, the boundary domains between leucosome and melanosome are generally lost. The more tightly spaced the melanosome and leucosome domains are, the higher the material loss from separating the two by cutting. Thus, there are a number of reasons why the quantitative chemical relations between leucosome, melanosome and bulk rock may be artificially (and unintentionally) skewed for some elements, and particularly those that have similar concentrations in the M and L fractions. Interestingly, though, the trace elements appear to be far less sensitive in that respect (as discussed below).

SiO_2, TiO_2, Al_2O_3 and MgO are distinctly enriched in the melanosome relative to the leucosome. This is also true for CaO and Na_2O, with the exception of sample KL2. FeO, MnO, K_2O and P_2O_5 are enriched in the leucosome. The vein-type leucosome can be seen to have a distinctly different composition compared to the other leucosomes of the dataset. It has significantly higher concentrations of SiO_2 and K_2O, with lower concentrations of Al_2O_3, MgO

and CaO. The two samples where leucosomes and melanosomes have not been separated (KL 20 and 25) behave quite similar to the other bulk migmatite samples apart from a significantly lower TiO_2 content and a slightly higher Al_2O_3 content.

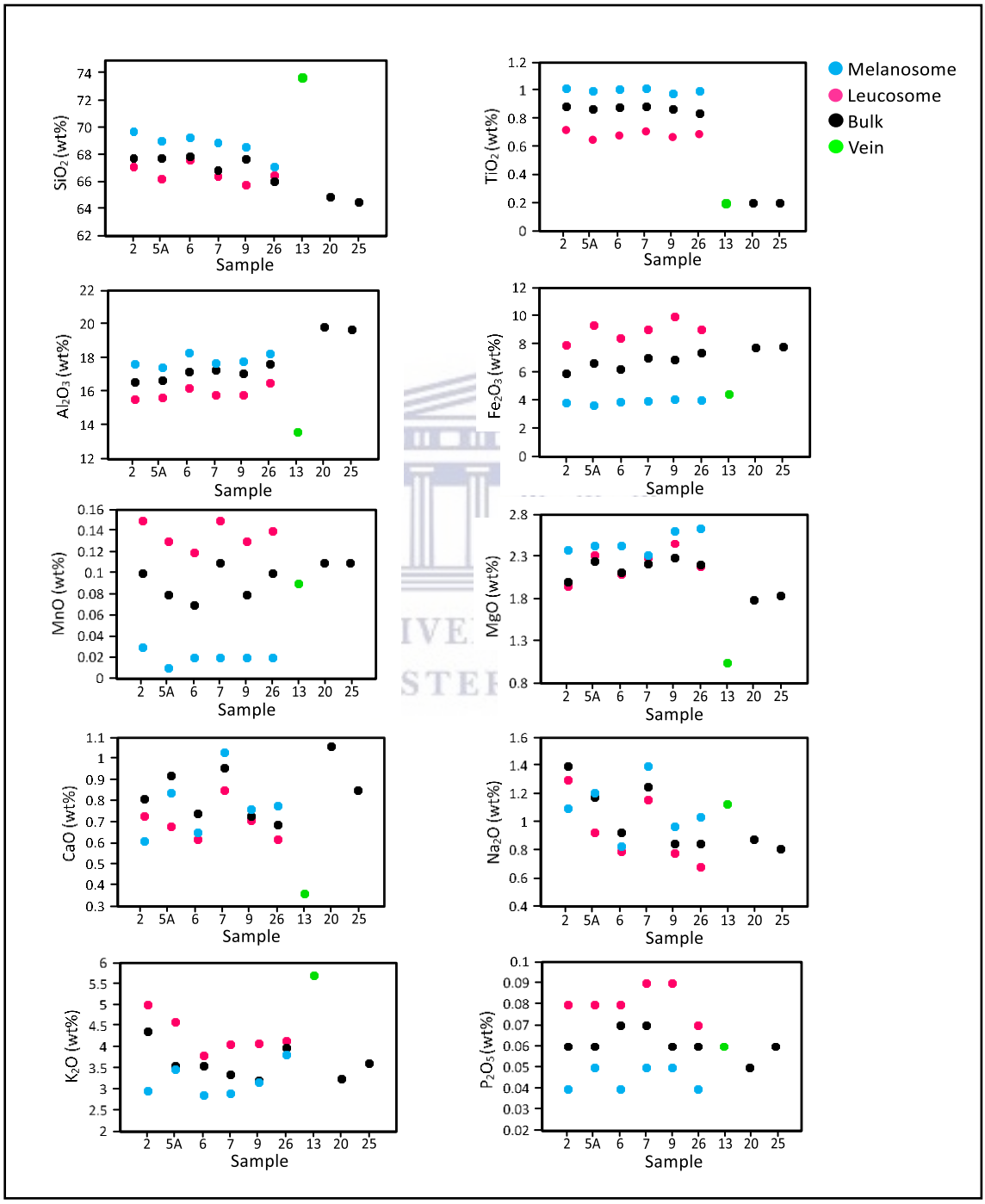

Figure 21: *Major element variation diagrams displaying differences in major element abundances for the leucosomes, melanosomes, bulk migmatite samples as well as the vein-type leucosome.*

5.3.2 Trace elements

Variation in trace element abundances between the different sample groups are depicted graphically in Figures 22 and 23. As discussed before, the separation of the bulk migmatite into melanosome and leucosome, without significant amounts of melt leaving the system, should result in the bulk sample data plotting between the melanosome and leucosome. The trace elements generally follow this expectation in a regular manner. There are, however, a few exceptions, which is due to similar reasons mentioned with regards to major oxide inconsistencies in element abundance between the leucosomes, melanosomes and bulk migmatite datasets. Figure 22 shows the enrichment of Zr, Nb, Zn and Cs in the melanosome and Figure 23 illustrates the clear enrichment of La, Nd, Sm, Y, Yb and Lu in the leucosome. The vein-type leucosome again shows major chemical differences to the fabric-parallel leucosomes as it has significantly lower Nb, La, Nd and Sm content as well as slightly higher Cs content. The vein-type leucosome also exhibits significantly higher concentrations of Zr than the fabric-parallel leucosomes.

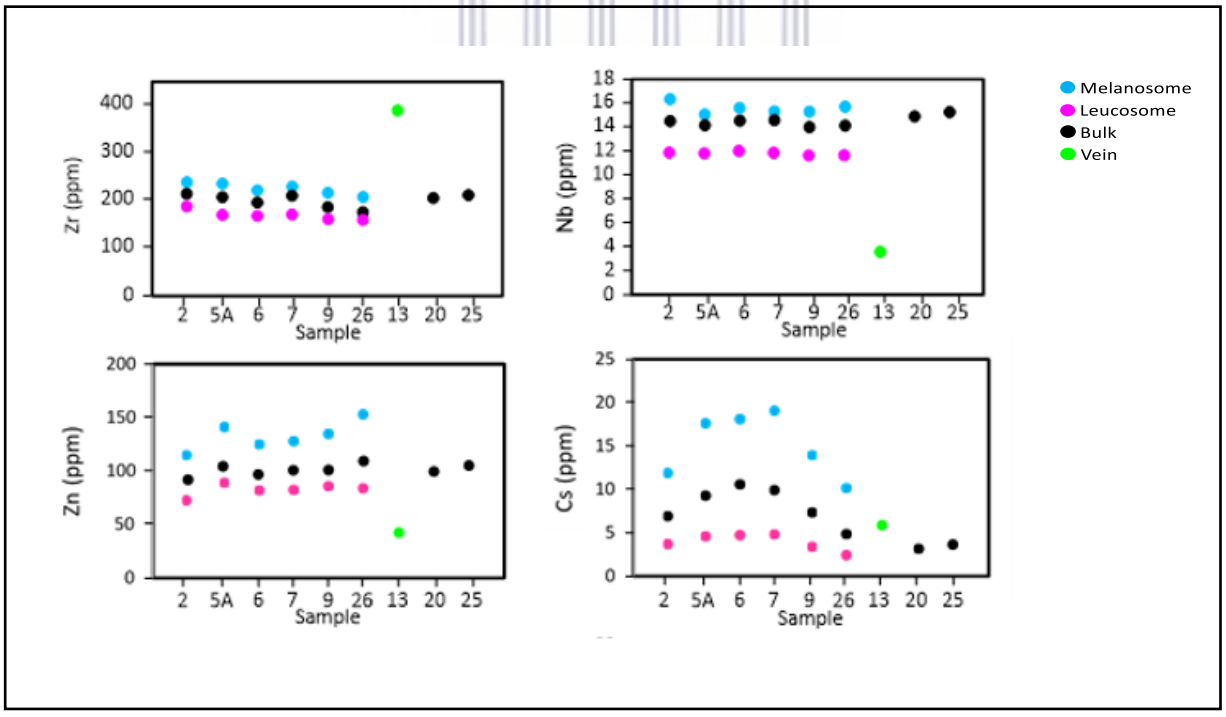

Figure 22: *Trace element variation diagrams displaying differences in trace element for the leucosomes, melanosomes, bulk migmatite samples as well as the vein type leucosome. Elements enriched in the melanosome are displayed here*.

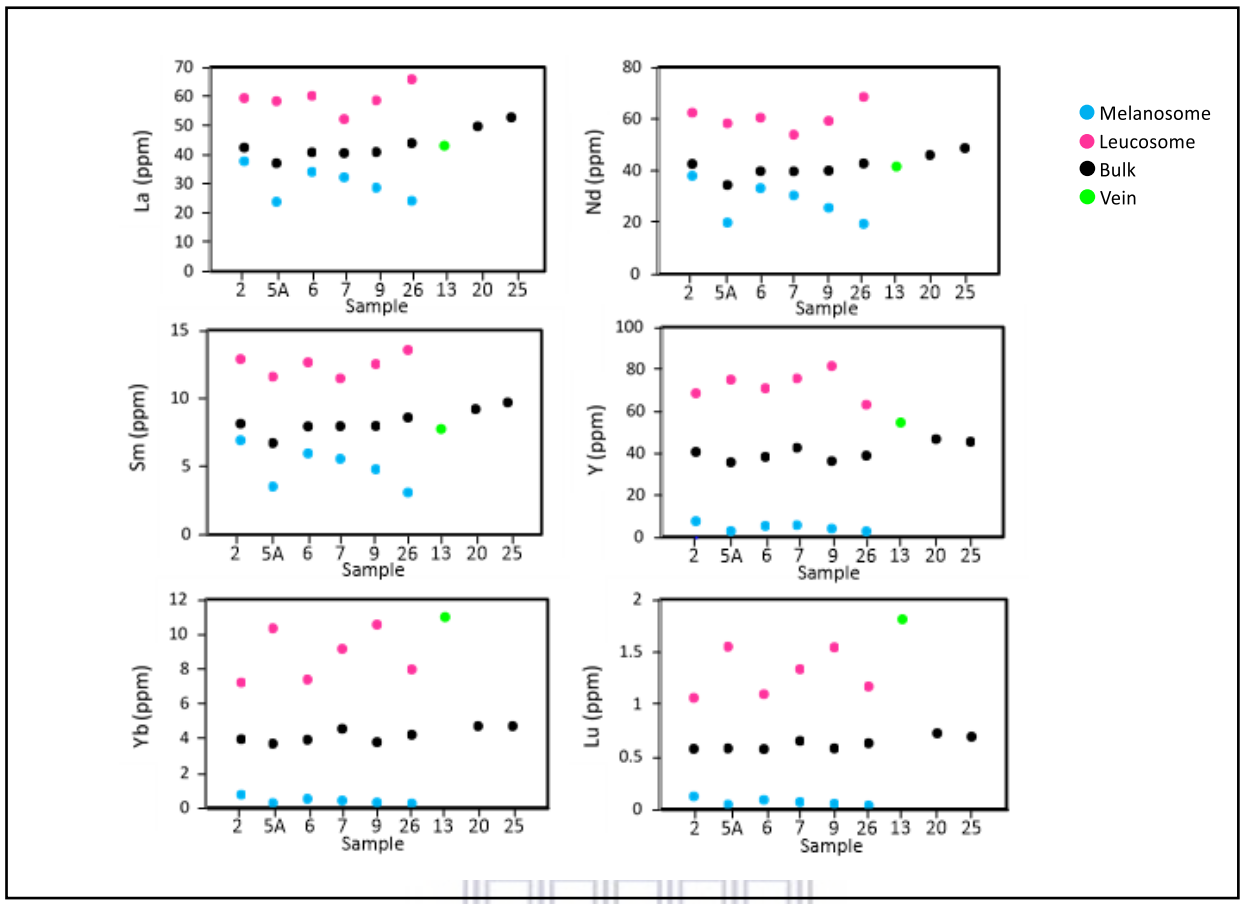

Figure 23: *Trace-element variation diagrams displaying differences in trace element abundances for the leucosomes, melanosomes, bulk migmatite samples as well as the vein-type leucosome. Elements enriched in the leucosome are displayed here.*

The leucosomes, melanosomes, bulk migmatite and vein-type leucosomes are plotted together on primitive mantle (PM)-normalized (McDonough and Sun, 1995) spider and REE diagrams in order to further assess elemental variations between the four sample groups. The diagrams illustrate, importantly, the bulk rock falling between that of the leucosome and melanosome, as expected. With respect to the spider diagram (Figure 24), there is distinct enrichment in the Large Ion Lithophile Elements (LILE) with respect to the High Field Strength Elements (HFSE) throughout the sample set. In the leucosome set there are slight enrichments in Th and Pb as well as slight depletions in Zr and Eu. There is a more noticeable depletion in Sr with a significant Nb-Ta trough. With respect to the bulk sample set, as previously mentioned, there are slight depletions in Ba, Zr, Eu and Ti with significant depletions in Nb, Ta and Sr. Slight enrichments are seen in Th and Pb.

The melanosomes behave largely similarly to both the leucosome and bulk as seen by the relatively similar patterns they exhibit. There are slight differences, for example, the melanosomes are enriched in Cs and somewhat depleted in Sm compared to the bulk and leucosome sets. Other than those differences they display almost an identical pattern on the spider diagram to that of the leucosome. There is, however, a significantly noticeable difference, this being the considerable depletion of the elements Dy – Y – Yb – Lu relative to that observed in the leucosome and bulk sets. The quartzo-feldspathic vein-type leucosome behaves differently to the rest of the samples. This is evident by a much more significant Nb-Ta trough, a slight enrichment in Zr and noticeably higher concentrations of Yb and Lu. There is also enrichment in Pb and significant depletions in Sr and Ti.

The REE diagram (Figure 25) displays the pattern of the bulk migmatite samples plotting between the leucosome and melanosome much clearer than the spider diagram. The leucosomes are enriched in the LREE relative to the HREE, evident from $(La/Lu)_{PM}$ values of 3.94 – 5.90. There is a strong negative Eu anomaly as $(Eu/Eu^*)_{PM}$ values fall between 0.35 and 0.49. The HREE exhibit relatively flat patterns as $(Gd/Lu)_{PM}$: 0.89 – 1.43, whilst the LREE display a greater degree of fractionation with $(La/Sm)_{PM}$: 2.88 – 3.15. The melanosomes behave slightly differently. This is evident from $(La/Lu)_{PM}$ values between 32.43 and 72.13, illustrating a severe depletion in the HREE. $(Eu/Eu^*)_{PM}$ values of the melanosomes show both negative and positive anomalies as values which range between 0.54 and 1.61. Both the LREE and the HREE exhibit moderate to strong degrees of fractionation as $(La/Sm)_{PM}$ and $(Gd/Lu)_{PM}$ have values ranging between 3.41 – 4.94 and 4.22 – 6.27, respectively. As for the quartzo-feldspathic vein, there is moderately strong LREE fractionation ($(La/Sm)_{PM}$:3.49). The HREE exhibit a positively sloping pattern as $(Gd/Lu)_{PM}$: 0.45. It has a negative Eu anomaly $(Eu/Eu^*)_{PM}$: 0.75), as well as LREE enrichment, relative to the HREE, as it has a $(La/Lu)_{PM}$ of 2.49. The bulk migmatite sample is discussed in great detail earlier in the chapter.

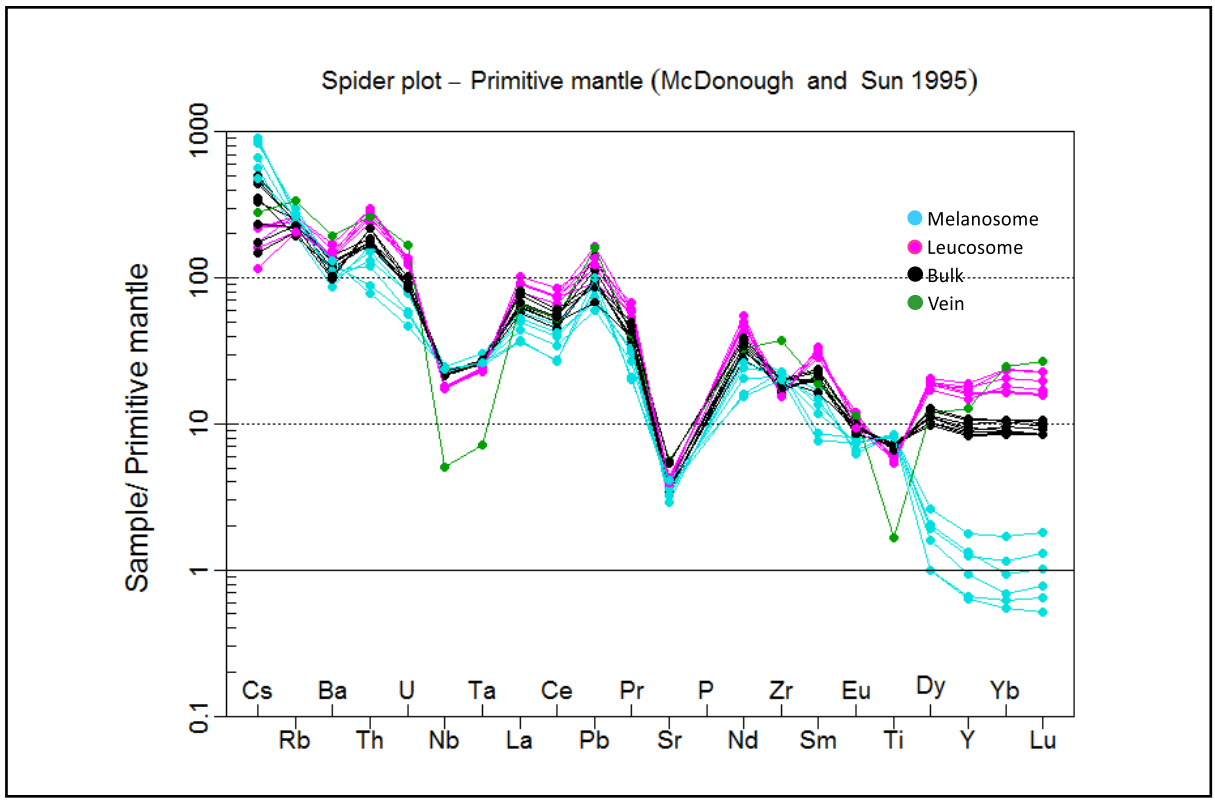

Figure 24: *Primitive-mantle normalized spider diagram, normalized to values of McDonough and Sun (1995).*

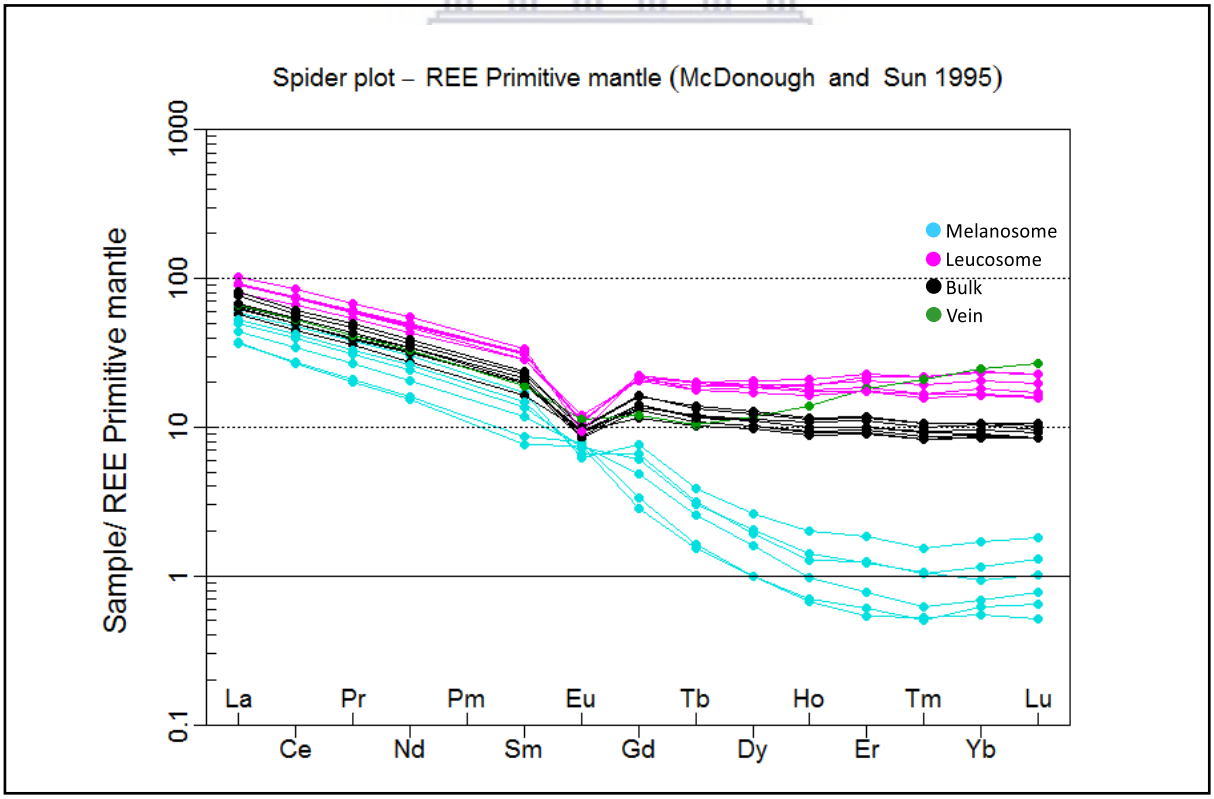

Figure 25: *Primitive-mantle normalized rare earth element plot, normalized to values of McDonough and Sun (1995).*

5.3.3 Quantifying element partitioning between leucosomes and melanosomes

The geochemical data demonstrates that many elements display a distinct preference for either the melanosome or the leucosome (Figures 21 – 25). These elements are enriched in one of the two segregations relative to the bulk migmatite composition, and depleted in the other. This 'preference' for a particular segregation can be quantified by what this study describes as a Bulk Distribution Coefficient (D) where D = element in melanosome/element in leucosome.

*with **D = 1** meaning there is equal distribution of an element between the leucosome and melanosome, **D > 1** meaning the element has a preference for or is more abundant in the melanosome and **D < 1** illustrating an elements preference for the leucosome.*

This is not intended to substitute for the more traditional mineral-melt partition coefficients, which is described as the equilibrium distribution of an element between a mineral and a melt (Rollinson, 1993). As mineral analyses are not available for this study, mineral-melt partition coefficients cannot be properly quantified here, and, importantly, the leucosomes cannot be taken to represent a melt fraction, due to the presence of abundant garnet in these leucosomes. Much, if not all, of this garnet may never have been part of a melt, but is rather considered to be a peritectic phase in the anatectic melt.

Thus, the bulk partition coefficient, as defined here, is used in conjunction with mineral/melt partition coefficient data from literature (Rollinson, 1993 and Bea et al., 1994) to explain why certain elements prefer the melanosome or leucosome segregations. Apart from the melt phase, the mineralogical composition (obtained from microscopic-petrographic analysis) is considered a primary control on the element fractionation, depending on which minerals most likely host particular minor and trace elements. In addition to mineral-melt element distribution data, published trace element data for the main minerals under discussion have been considered (Deer et al., 1997a, 1997b, 2001; Fleet, 2003).

Table 7 shows the calculated bulk distribution coefficients for Ti, Mn, Sc, Zn, Rb, Sr, Y, Zr, Nb, Cs, Ba, Pb, the REE and Th. A general preference for the melanosome is shown by Ti, Zn, Rb, Zr, Nb and Cs, which all have D values greater than 1. Mn, Sc, Sr, Y, Ba, Pb, Th and the REE show D values less than and thus are more abundant in the leucosome.

The moderate to strong preference for the melanosome, shown by the elements Ti, Zn, Nb and Cs, is largely due to their affinity to biotite (Bea et al., 1994). Biotite is hosted almost exclusively in the melanosome. The amount of Zr in either the leucosome or melanosome is most likely a reflection of the amount or zircon in either segregation, rather than being controlled by any of the main phases. Mn, the HREE as well as Sc and Y display a strong preference for the leucosome which is attributed to the presence of garnet therein. The HREE have a well-documented affinity for partitioning in to garnet during melting (Rollinson, 1993). Sr and Ba display weak and moderate preferences, respectively, for the leucosome, most likely a result of their affinity for orthoclase, which is concentrated in the leucosome. Since Sr is also incorporated in plagioclase, the two feldspars "compete" for Sr, which explains a fluctuating D close to 1. Pb has a moderate preference for the leucosome, due to its affinity for orthoclase. While Rb is also incorporated in orthoclase, the weak preference for the melanosome in most samples is seen as resulting from Rb being readily accommodated in biotite as well. Th is incorporated into orthoclase, which explains the moderate preference for the leucosome. The LREE (La, Ce, Pr, Nd, Sm, Eu and Gd) generally display moderate preferences for the leucosome. Orthoclase has the largest effect on these elements (Bea et al., 1994) and the moderate preference of the LREE for the leucosome can be explained by orthoclase being present in both segregations, just slightly more abundant in the leucosome.

The abundance of certain elements in either the leucosome or melanosome segregations is thus attributed to the element's affinity for a particular mineral. Elements are either enriched or depleted in a particular segregation and where the bulk partition coefficients are close to 1 there is typically mineral phases in either segregation competing to host the element.

Table 6: Minor (Ti and Mn) (wt.%), Trace (ppm) and REE (ppm) element abundances in the leucosomes and melanosomes. L - Leucosome, M – Melanosome, D - Distribution Coefficient.

Sample	Ti	Mn	Sc	Zn	Rb	Sr	Y	Zr	Nb
KL2 L	0.72	0.15	24.4	72.5	161	83	68.5	189	11.8
KL2 M	1.02	0.03	3.8	115	118	57.4	7.6	241	16.3
D = M/L	1.42	0.20	0.16	1.59	0.74	0.69	0.11	1.28	1.38
KL5A L	0.65	0.13	27.8	88.9	158	85.42	75.1	168	11.7
KL5A M	1	0.01	2.3	141	181	71.5	2.8	237	15.0
D = M/L	1.54	0.08	0.08	1.59	1.14	0.84	0.04	1.41	1.28
KL6 L	0.68	0.12	26.5	81.8	133	83.6	70.8	167	11.9
KL6 M	1.01	0.02	3.2	125	161	63.7	5.3	224	15.6
D = M/L	1.49	0.17	0.12	1.53	1.21	0.76	0.08	1.34	1.31
KL7 L	0.71	0.15	28.8	82.4	145	74.1	75.6	171	11.8
KL7 M	1.02	0.02	3.0	128	166	64.7	5.7	232	15.2
D = M/L	1.44	0.13	0.10	1.55	1.14	0.87	0.08	1.36	1.30
KL9 L	0.67	0.13	32.3	85.9	123	81.7	81.5	161	11.5
KL9 M	0.98	0.02	2.5	135	145	71.3	4.0	218	15.3
D = M/L	1.46	0.15	0.08	1.57	1.18	0.87	0.05	1.35	1.33
KL26 L	0.69	0.14	24.7	83.9	124	78.4	63.1	161	11.5
KL26 M	1	0.02	2.4	153	159	81.3	2.7	209	15.6
D = M/L	1.45	0.14	0.10	1.82	1.28	1.04	0.04	1.30	1.36

Table 7: Continued

Sample	Cs	Ba	Pb	La	Ce	Pr	Nd	Sm	Eu
KL2 L	3.7	1018	24.5	59.4	127	15.6	62.4	12.9	1.6
KL2 M	11.9	574	14.0	37.7	79.9	9.7	37.9	6.9	1.0
D = M/L	3.22	0.56	0.57	0.63	0.63	0.62	0.61	0.54	0.58
KL5A L	4.6	1137	20.3	58.3	122	14.8	58.3	11.6	1.8
KL5A M	17.6	820	12.6	23.8	45.9	5.3	19.9	3.5	1.2
D = M/L	3.86	0.72	0.62	0.41	0.38	0.36	0.34	0.30	0.67
KL6 L	4.7	922	17.3	60.1	127	15.3	60.5	12.6	1.7
KL6 M	18.1	648	10.1	34.1	70.6	8.4	33.1	5.9	1.0
D = M/L	3.83	0.70	0.58	0.57	0.56	0.55	0.55	0.47	0.61
KL7 L	4.8	919	17.7	52.2	111	13.6	53.8	11.5	1.7
KL7 M	19.1	644	11.1	32.2	66.3	7.8	30.4	5.6	1.1
D = M/L	3.97	0.70	0.63	0.62	0.60	0.58	0.56	0.48	0.67
KL9 L	3.4	945	13.9	58.6	123	15.0	59.3	12.5	1.7
KL9 M	13.9	736	9.0	28.6	57.1	6.8	25.6	4.8	1.2
D = M/L	4.12	0.78	0.64	0.49	0.46	0.45	0.43	0.38	0.68
KL26 L	2.4	959	18.5	65.9	141	17.2	68.6	13.5	1.5
KL26 M	10.1	855	15.1	24.2	45.0	5.1	19.4	3.1	1.2
D = M/L	4.19	0.89	0.82	0.37	0.32	0.30	0.28	0.23	0.79

Table 7: Continued

Sample	Gd	Tb	Dy	Ho	Er	Tm	Yb	Lu	Th
KL2 L	12.1	1.9	12.6	2.6	7.6	1.07	7.2	1.1	21.1
KL2 M	4.1	0.4	1.8	0.30	0.80	0.11	0.75	0.12	13.3
D = M/L	0.34	0.20	0.14	0.11	0.11	0.10	0.10	0.11	0.63
KL5A L	11.1	1.8	12.6	2.8	9.6	1.5	10.3	1.5	23.5
KL5A M	1.8	0.16	0.7	0.10	0.27	0.03	0.27	0.04	7.1
D = M/L	0.16	0.09	0.05	0.04	0.03	0.02	0.03	0.03	0.30
KL6 L	12.1	2.0	13.0	2.6	8.1	1.1	7.4	1.10	22.0
KL6 M	3.6	0.31	1.3	0.19	0.54	0.07	0.51	0.09	12.0
D = M/L	0.30	0.16	0.10	0.07	0.07	0.06	0.07	0.08	0.55
KL7 L	11.5	1.9	13.0	2.9	9.0	1.3	9.1	1.3	18.9
KL7 M	3.3	0.30	1.4	0.21	0.53	0.07	0.41	0.07	10.4
D = M/L	0.29	0.16	0.11	0.07	0.06	0.05	0.05	0.05	0.55
KL9 L	11.6	2.0	13.8	3.1	9.9	1.5	10.6	1.5	20.7
KL9 M	2.7	0.26	1.1	0.14	0.34	0.04	0.3	0.05	9.6
D = M/L	0.23	0.13	0.08	0.05	0.03	0.03	0.03	0.03	0.46
KL26 L	11.8	1.8	11.4	2.4	7.6	1.1	8.0	1.2	24.0
KL26 M	1.5	0.15	0.67	0.10	0.24	0.04	0.24	0.04	6.3
D = M/L	0.13	0.09	0.06	0.04	0.03	0.03	0.03	0.03	0.26

5.4 Determination of leucosome and melanosome proportions from element distribution

For the samples for which leucosome, melanosome and bulk geochemical data are available (KL2, 5A, 6, 7, 9 and 26), the weight proportions (wt%. prop.) of leucosomes and melanosomes have been calculated by using the fractionation of elements between leucosome and melanosome. The first step involved calculating the proportion of leucosome present. This was achieved by subtracting the melanosome value of a particular element or oxide for a particular sample from the bulk value of that same sample. This was then divided by the result of subtracting the melanosome from the leucosome value of that same sample and element or oxide.

Leucosome prop. (wt. prop in %) = 100% (element in bulk rock – element in melanosome)/ (element in leucosome – element in melanosome)

The melanosome proportion was then calculated as:

Melanosome prop. + 100 – leucosome prop. (wt %. prop)

Elements which were used were selected on the basis of which ones in particular show a substantial difference between leucosome, melanosome and bulk values. If the difference is too close or values too similar the calculation would not yield accurate results, thus elements with distinct fractionation between the leucosome and melanosome were chosen. This includes the major oxide Fe_2O_3. Trace elements selected are Sc and Y as well as the HREE: Gd, Tb, Dy, Ho, Er, Tm, Yb and Lu. Average leucosome and melanosome proportions for the six samples are displayed in Table 8. The average overall leucosome proportion for the six samples is 49.5% whilst the overall melanosome proportion is 50.5%.

Table 7: Leucosome and melanosome proportions calculated using elemental concentrations, B – Bulk migmatite, L - Leucosome, M – Melanosome, S.D – Standard Deviation (calculated for leucosomes only), wt% prop. – Weight percent proportions.

	KL2		KL5A		KL6		KL7		KL9		KL26	
	wt%	wt% prop.	wt%	wt% prop.	wt%	wt% prop.	wt%	wt% prop.	wt%	wt% prop.	wt%	wt% prop.
Fe_2O_3 B	5.97		6.66		6.23		7.02		6.93		7.38	
Fe_2O_3 L	7.94	51.8	9.36	52.4	8.48	51.0	9.09	59.6	9.99	48.1	9.08	66.3
Fe_2O_3 M	3.85	48.2	3.69	47.6	3.89	49.0	3.96	40.4	4.09	51.9	4.03	33.7
Sc B	14.94		14.41		14.80		17.38		15.11		16.37	
Sc L	24.41	54.1	27.80	47.5	26.46	49.8	28.81	55.7	32.26	42.3	24.72	62.6
Sc M	3.79	45.9	2.28	52.5	3.24	50.2	3.00	44.3	2.54	57.7	2.36	37.4
Y B	40.53		35.63		38.22		42.62		36.24		38.80	
Y L	68.46	54.1	75.05	45.4	70.82	50.2	75.59	52.8	81.51	41.6	63.10	59.8
Y M	7.59	45.9	2.84	54.6	5.34	49.8	5.69	47.2	4.00	58.4	2.72	40.2
Gd B	7.69		6.29		7.13		7.37		7.15		7.76	
Gd L	12.12	44.6	11.08	48.3	12.11	41.6	11.48	49.5	11.57	50.4	11.75	60.9
Gd M	4.12	55.4	1.81	51.7	3.58	58.4	3.34	50.5	2.66	49.6	1.55	39.1
Tb B	1.17		1.01		1.08		1.18		1.08		1.14	
Tb L	1.95	50.4	1.76	52.8	1.97	46.5	1.88	55.7	1.98	47.5	1.76	61.5
Tb M	0.38	49.6	0.16	47.2	0.31	53.5	0.30	44.3	0.26	52.5	0.15	38.5
Dy B	7.41		6.63		6.94		7.68		6.92		7.43	
Dy L	12.57	52.3	12.60	50.0	12.96	48.3	13.02	54.1	13.85	45.8	11.45	62.7
Dy M	1.75	47.7	0.67	50.0	1.30	51.7	1.38	45.9	1.08	54.2	0.67	37.3
Ho B	1.49		1.32		1.39		1.60		1.36		1.49	
Ho L	2.58	52.2	2.81	44.8	2.64	48.8	2.87	52.4	3.11	40.9	2.45	59.4
Ho M	0.30	47.8	0.10	55.2	0.19	51.2	0.21	47.6	0.14	59.1	0.10	40.6
Er B	4.39		3.98		4.23		4.81		4.00		4.42	
Er L	7.63	52.6	9.58	39.8	8.10	48.7	9.01	50.4	9.88	38.4	7.57	57.0
Er M	0.80	47.4	0.27	60.2	0.54	51.3	0.53	49.6	0.34	61.6	0.24	43.0
Tm B	0.63		0.57		0.58		0.68		0.57		0.64	
Tm L	1.07	54.0	1.48	36.9	1.13	48.5	1.32	48.9	1.48	36.7	1.14	54.8
Tm M	0.11	46.0	0.03	63.1	0.07	51.5	0.07	51.1	0.04	63.3	0.04	45.2
Yb B	3.94		3.70		3.92		4.54		3.78		4.21	
Yb L	7.21	49.4	10.33	34.1	7.38	49.6	9.14	47.3	10.55	33.9	7.97	51.3
Yb M	0.75	50.6	0.27	65.9	0.51	50.4	0.41	52.7	0.30	66.1	0.24	48.7
Lu B	0.58		0.58		0.57		0.65		0.58		0.63	
Lu L	1.06	48.2	1.55	35.5	1.10	48.2	1.34	45.9	1.54	35.4	1.17	52.3
Lu M	0.12	51.8	0.04	64.5	0.09	51.8	0.07	54.1	0.05	64.6	0.04	47.7
Ave L		51.2		44.3		48.3		52.0		41.9		59.0
Ave M		48.8		55.7		51.7		48.0		58.1		41.0
S.D		2.9		6.7		2.5		4.1		5.5		4.7

5.5 Density estimates: melt, magma and residue

Densities of melts and rocks can be calculated from composition data. As mineral compositions had not been determined for this project, only relatively crude estimates could be made here. The term "magma", as used here, refers to melt plus any solid material carried in it, which, in the case of this study, is garnet. Magma and melanosome densities were estimated by using proportions of minerals in samples as obtained through microscopic – petrographic analysis. For the magma densities the following calculation was used: $(\frac{Quartz + Feldspar\ vol.\ proportion}{100})2.4 + (\frac{Garnet\ vol.\ proportion}{100})4.17$

**2.4g/cm³ - average density of granitic melts*

**4.17g/cm³ - density of almandine-dominated garnet*

With respect to the solid melanosome, the density estimate was obtained using a similar equation: $\frac{Mineral\ X\ vol.\ proportion}{100} * (density\ of\ mineral\ X)$. This was done for all the constituent minerals of the melanosome (Qtz, Or, Pl, Bt, Sil, Crd etc.). The mineral model compositions of the mafic components (Crd and Bt) had been chosen such that they correspond to the Mg/Fe ratio in the rock analysis; oligoclase composition has been considered for plagioclase. These values were then added up to estimate the overall density of the melanosome.

Accordingly, the density of the magma, calculated for seven samples range between 2.69 and 2.8 g/cm³. For the melanosomes it ranges between 2.7 and 3 g/cm³. Thus, this exercise suggests that magmas and melanosomes display very similar densities with the melanosomes just being slightly higher. The fact that the magma has such a similar density to the residual rock, in contrast to a pure melt of about 2.4 g/cm^3, is due to the garnet content in the magma. This makes a substantial difference to the density contrast.

6. Discussion

6.1 Migmatite protolith

Bulk migmatite samples of this study display evidence for having a pelitic origin if compared with Ca-poor pelitic and metapelitic reference compositions (NASC, PAAS, and others; Figures 13 and 18). The average melanosome composition (Figure 13) plots away from the cluster of reference data and the bulk migmatite samples. This can be taken as the effect of thorough modification of rock composition by the extraction of a melt component. The melanosomes are therefore interpreted to be largely melt - depleted residual compositions. Considering the option of an externally derived leucosome that in combination with a residual rock would produce a pelitic bulk composition (as an injected migmatite), this is regarded as highly unlikely.

The data also argues against any significant partial extraction of melt. The bulk samples do not display any trends which suggest that the compositions have shifted off the average pelite field as a result of subtracting a melt of granitic composition. The migmatites are interpreted to represent essentially original protolith compositions, despite relatively effective separation of melt and residuum at the hand specimen scale. The leucosome compositions are also indicative of pelitic sources (Figures 14A and 15) and plot within the reference cluster for leucosomes formed via dehydration melting reactions (Figure 14B).

6.2 Geochemical relationships between leucosome and melanosome

Bulk rock distribution coefficients highlight in which segregation a particular element is enriched. Certain elements prefer the leucosome and some the melanosome. This is largely controlled by the mineralogical composition of the leucosome and melanosome, and mineral-specific distribution coefficients, either between mineral and melt, or between minerals equilibrating at subsolidus conditions. Various elements are fractionated between leucosomes and melanosome, such that they are enriched in either segregation and correspondingly depleted in the other. Other elements do not show a distinct prefence (values close to 1); this may be due to competing phases in the leucosome and melanosome segregations (see under section 4.3.3). An example of strong fractionation is the HREE enrichment in the leucosome and depletion of HREE in the melanosome (due to the garnet

being contained in the leucosome). This also points to a closed-system behaviour at the outcrop scale. Mineral – melt partition data from Rollinson (1993) and Bea et al. (1994) provide insight into which mineral is the likely host of which elements. This cannot be solely used as the explanation for element distribution, as other factors such as chemical equilibration after solidification must also be considered as elements readjust themselves once the components which were part of the melt have solidified.

The abundance of garnet causes the leucosomes (of this study) to have a more mafic composition than the melanosome, which appears to be inconsistent with established views of partial melting. A visual representation of the effect garnet has is displayed in Figure 16. Garnet also significantly increases the density of the leucosome, which was estimated to be between 2.7 g/cm^3 and 2.8 g/cm^3 (leucosome calculated as magma, i.e., melt plus garnet), in contrast to pure granitic melt having a density of approximately 2.4 g/cm^3. The density of the melanosome was calculated to be between 2.7 g/cm^3 and 3 g/cm^3. Hence, there would have been very little contrast in the density of the leucosome and melanosome. This could be one of the reasons why the melt had not segregated further and migrated away from the residuum before cooling and solidification.

6.3 Evidence for in situ anatexis

Textural observations in the field and at the hand specimen scale illustrate a well-defined parallel interlayering of leucosomes and melanosomes (Figures 5, 7 and 8); this texture is termed ‘stromatic’ and is strictly associated with metatexite migmatites (Sawyer, 2008). This textural feature has been noted by various authors as a defining characteristic of neosomes (leucosomes and melanosomes) formed by in situ anatectic processes (Waters and Whales, 1984; Brown, 1994). The two segregations seem to have a fairly regular distribution and similar volumetric proportions. The leucosomes, when studied in the samples which are cut perpendicular to the “L” fabric, display a patchy appearance, whereby they appear as semi-rounded patches enclosed in a melanosome matrix (Figures 7A and 7B). Waters and Whalen (1984) describe this patchy and enclosed nature as a textural indicator of in-situ partial melting whereby the melt has not left the system but crystallised in place. Brown (1994) also suggests that stromatic migmatites are a product of in situ melting by stating that a melt that

cannot escape from a system will remain in place, and crystallize as a migmatite with a stromatic structure. Further macroscopic textural observations include the fact that the leucosomes are relatively strain-free and exhibit a granoblastic texture compared to the adjacent melanosomes. This is seen as evidence for in situ formation (Jung et al., 1999).

Post crystallisation deformation typically leaves minimal evidence for crystallisation from a melt. Undulose extinction and lobate grain boundaries in quartz are observed and occur as a result of sub-solidus plastic deformation. This typically removes most of the evidence for crystallisation from a melt, common of migmatites in regional metamorphic terranes (Sawyer, 2008). There is, however, a remaining indicator of crystallisation from a melt, such as straight faces of quartz with K-feldspar. Most quartz exhibit lobate grain shapes and thus have relatively curved grain boundaries. There are, however, a few remaining sites (after sub-solidus plastic deformation) where quartz and K-feldspar (orthoclase) share straight crystal faces. This provides microstructural evidence for crystallisation from a melt (Sawyer, 2008). Further observations at the thin section scale reveal that all the minerals involved in the assumed melting reaction (Bt + Sil + Qtz → Grt + Crd + Kfs + melt) are present in the leucosomes and melanosomes. Expectedly, one finds Grt and Kfs, as well as the solid products of melting, in the leucosome. Garnets also contain rounded inclusions of quartz and biotite which can be interpreted as remnants of the original reactant minerals. The presence of cordierite in the leucosome is restricted to rims of the garnet grains. It is, however, abundant in the melanosome. If cordierite in the melanosome is a product of the melting reaction, the melanosome is not simply a residuum in the strict sense.

This interpretation coincides with the model of formation of an in situ migmatite as proposed by White et al. (2004). They suggest that garnet forms initially (as the result of the breakdown of sillimanite and biotite) at favourable sites which is followed by K-feldspar and melt forming around the garnet while cordierite begins to form in the adjacent melanosome. It needs to be pointed out, though, that the White et al. (2004) model is based on rock composition that are distinctly higher in Fe/Mg than the samples of this study. It is therefore likely that cordierite was present in the Kliprand rocks at subsolidus conditions already. In that case, at least part of the cordierite in the melanosome is truly residual, while taking into account chemical re-equilibration at anatectic conditions. Hence, only further quantitative thermodynamic modelling of the KL samples would reveal the proportion of residual versus anatexis-related

cordierite. Garnet grains form large porphyroblasts which are commonly intergrown with quartz and surrounded by K-feldspar (orthoclase). This is a common microstructure in neosomes formed as a result of biotite dehydration reactions and common of neosomes with an in situ origin (Sawyer, 2008). Powell and Downes (1990) attribute the presence of mafic (garnet) porphyroblasts to incongruent melting reactions wherein hydrous minerals (such as biotite) are consumed. Biotite has not been fully consumed, however, as it is still present in the melanosome.

The contact boundary between leucosomes and melanosomes at the microscopic scale can be used to infer an in situ or an injected origin of the melt. Sharp, well defined, contacts are typical of injected melts and the opposite is true of melts which crystallised in situ (Saywer, 2008). The boundaries observed between the leucosomes and melanosomes are irregular (characteristic of in situ melts) and often times hard to distinguish due either segregation having similar mineralogy. The leucosomes also do not seem to exhibit any magmatic foliations or any microstructure formed as a result of magmatic flow.

The vein-type leucosome exhibits different microscopic features (compared to the stromatic leucosome), such as a significantly larger average grain size, much lower garnet content and noticeably fewer opaque minerals. With respect to the contact between the vein-type leucosome and the melanosome, it is a lot more distinct. These factors tend to suggest that it could be unrelated to the stromatic leucosomes and probably externally derived. Of the vein samples studied none contain hercynite. This also brings into question its age of emplacement. Could it then perhaps be a later generation of melt? Further age studies could answer this question.

The pelitic origin, as well as the fact that the leucosome and melanosome compositions combine to form a bulk migmatite composition presents evidence that the leucosomes are a product of an in situ anatectic process and the melanosomes are what is left after the melt plus garnet had separated out. It must be noted that minor passive entrainment of residual phases from the melanosome into the leucosome cannot be excluded. This can only be resolved from thermodynamic phase equilibria modelling.

6.4 Volumetric relationships

The proportions of leucosome versus melanosome have been determined by using elements that are most strongly fractionated between leucosome and melanosome (Table 8). This reveals that the segregations are relatively similarly proportioned. The leucosome constitutes between 42– 59% of the rock, with the melanosome making up between 41% and 58%. Thus, the proportions are relatively consistent within a narrow range across the sample range, and systematic differences between samples are assumed to reflect local variations in pre-anatectic bulk rock composition. This provides additional evidence pro in situ versus externally derived leucosomes, as injected melts would be far more heterogeneously distributed, and thus create a large range of leucosome/host rock proportions.

The migmatite system investigated in this study behaves differently to previously studied migmatites formed in comparable environments (see Sawyer, 2008). What is observed in this study is a leucosome that is more mafic than the residuum, because of the large garnet content, a residuum with a higher SiO_2 content than the melanosome, which is uncharacteristic. Further modelling should provide insight into why the migmatites studied here exhibit these characteristics.

The vein-type leucosome at first glance seems to be quite similar in terms of major-element geochemistry. However, trace-element data proves how different the vein-type leucosome is compared to the stromatic leucosomes. Even though only one vein sample has been geochemically analysed, the striking geochemical difference to the other leucosomes emphasize the contrast between the in situ types and the externally derived injected melts, which does not seem to have originated locally from the migmatites investigated in this study.

7. Conclusions

The samples studied for this project form part of the supracrustal Kamiesberg Group of the Bushmanland Subprovince. The migmatites that show a distinct, fairly regular, spaced distribution of leucosome and melanosome at hand specimen scale were found to occur in a restricted outcrop area surrounded by granites of the Spektakel Suite. Geochemically, the migmatite samples are metapelitic in character. The outcrop is located in the "upper granulite facies" part of the Bushmanland Domain where metapelites occur in association with other supracrustal lithologies including calc-silicate gneisses, quartzitic gneisses and semi-pelitic gneisses. High to possibly ultra-high metamorphic temperatures are confirmed by the occurrence of hercynite + quartz in the studied samples.

The main regional deformational event affecting these rocks is D_2 (~1.13 to ~1.06 Ga), forming the main foliation, which includes aligned biotite and sillimanite. Peak P-T conditions (~750°-870°C and 4.5 – 6 kbar) occurred around 1.03 Ga and resulted in incipient crustal anatexis. This produced fabric-parallel, garnet-bearing quartzo-feldspathic segregations through the biotite dehydration melting reaction: sillimanite + biotite + quartz → cordierite + garnet + K-feldspar + melt. All products and reactants of this reaction are hosted within the system. Elevated thermal gradients are evident by the presence of accessory hercynite.

The leucosomes formed in situ. The chemical relationship between the melanosomes and the foliation-parallel leucosomes indicates that the latter are not externally derived melts, in contrast to a cross-cutting melt vein with a distinctly different composition. There is also no evidence for any significant loss of melt. Thus, the surrounding melanosome represents the residuum after the magma had been extracted from the initial bulk rock. The melt did not migrate away from the site of anatexis, but accumulated within the system as strain free, elongate cigar-shaped lenses which define a macroscopic linear structure. The relatively consistent proportions of leucosome and melanosome provide supporting evidence for an in-situ formation of the leucosome. Injected melts would be expected to have a highly variable range of leucosome/melanosome proportions, compared to the relatively homogenous distribution of the leucosome segregations observed in this study. Furthermore, the leucosome and melanosomes combine to form a bulk rock that compares well with average pelitic compositions. It is highly unlikely that an externally derived melt would combine with

an unrelated host rock, even if that was residual in nature, such that the bulk migmatite corresponds to a pelitic composition. The two segregations have near-identical trace element patterns apart from the depletion of HREE in the melanosomes and the enrichment of these HREE in the leucosome. This distribution of the HREE is attributed to garnet which is concentrated in the leucosome. The abundance of garnet in the leuosome results in an uncharacteristically mafic leucosome. It also lowers the density contrast between the leucosome and melanosome significantly.

The distribution of the other elements between leucosome and melanosome is controlled by the minerals hosted in each segregation. The migmatite behaved as an essentially closed system where elements partitioned themselves at favourable sites between the two segregations, first in a melt-solid system under anatectic conditions and later under post-peak subsolidus conditions. There is no evidence for chemical modification of the migmatite system from external sources. The cross-cutting vein-type leucosome is an example of externally derived melt with a geochemical signature that is quite distinct from the in-situ leucosomes of the migmatite samples studied.

The metapelitic migmatite studied as part of this research has thus formed from biotite dehydration melting close to peak metamorphic conditions where a garnet-bearing leucosome was produced in situ and set in a residual matrix. The system experienced no significant loss of melt and the products and reactants of the partial melting process are preserved at the site of initial anatexis. Further insights into the anatectic process should be gained from mineral analyses of the mafic phases and feldspars in particular, and from thermodynamic modelling based on such analyses.

8. References

- Ague, J.J. (1991). Evidence for major mass transfer and volume strain during regional metamorphism of pelites, *Geology*, 19(8), 855 – 858.
- Altherr, F.F., Holl, A., Hegner, E., Langer, C., Kreuzer, H. (2000). High potassium, calc-alkaline I-type plutonism in the European Variscides: Northern Vosges (France) and Northern Schwarzwald (Germany). *Lithos*, 50(1-3), 51-73.
- Bailie, R., Armstrong, R. and Reid, D. (2007). Composition and single zircon U-Pb emplacement and metamorphic ages of the Aggeneys Granite Suite, Bushmanland, South Africa. *South African Journal of Geology*, 110(1), 87-110.
- Bailie, R., Abrahams, G., Bokana, R., van Bever Donker, J., Frei, D., Le Roux, P. (2019). The geochemistry and geochronology of the upper granulite facies Kliprand dome: comparison of the southern and northern parts of the Bushmanland Domain of the Namaqua Metamorphic Province, southern Africa and clues to its evolution. *Precambrian Research*, 330, 58–100.
- Bea, F., Pereira, M.D. and Stroh, A. (1994). Mineral/leucosome trace element partitioning in a peraluminous migmatite (a laser ablation-ICP-MS-study). *Chemical Geology,* 117, 291-312.
- Blignaut, H.J. (1977). Structural-metamorphic imprint on part of the Namaqua mobile belt in South West Africa. *Bulletin, Precambrian Research Unit*, vol. 23. University of Cape Town. 197 pp.
- Brown, M. (1994). The generation, segregation, ascent and emplacement of granite magma: the migmatite-to-crustally-derived granite connection in thickened orogens. *Earth Science Reviews,* 86, 83-130.
- Cameron, E.M. and Garrels, R.M. (1980). Geochemical composition of some Precambrian shales from the Canadian Shield, *Chemical Geology*, 28, 181-197.
- Cornell, D. and Pettersson, Å. (2007). Ion probe zircon dating of metasediments from the Areachap and Kakamas Terranes, Namaqua-Natal Province and the stratigraphic integrity of the Areachap Group. *South African Journal of Geology*, 110(4), 575-584.
- Cornell, D., Thomas, B., Moen, H.F.G., Reid, D.L., Moore, J.M., Gibson, R.L. (2006). The Namaqua-Natal Province. The Geology of South Africa. *Geological Society of South Africa*. 352-379.
- Deer, W.A., Howie, R.S., Zussman, J. (1997a). Rock-Forming Minerals, Volume 2A, Single-Chain Silicates, second edition. *Geological Society of London.*

- Deer, W.A., Howie, R.A., Zussman, J. (1997b). Rock-Forming Minerals, Volume 2B, Double Chain Silicates, second edition. *Geological Society of London.*
- Deer, W.A., Howie, R.A., Zussman, J. (2001). Rock-Forming Minerals, Volume 4A, Framework Silicates, second edition. *Geological Society of London.*
- Dewey, J., Robb, L. and Van Schalkwyk, L. (2006). Did Bushmanland extensionally unroof Namaqualand? *Precambrian Research*, 150 (3-4), 173-182.
- Diener, J.F.A., Thomas, R.J., Macey, P.H. (2017). Pan-African accretionary metamorphism in the Sperrgebiet Domain, Gariep Belt, SW Namibia, *Precambrian Research*, 292, 152–162.
- Dwivedi, S.B., Theunuo, K. (2013). Petrology and geochemistry of metapelites and basic granulites from Sonapahar region of Shillong Meghalaya Gneissic Complex, North East India. *Journal Geological Society of India*, 81, 755-766.
- Eglington, B. (2006). Evolution of the Namaqua-Natal Belt, Southern Africa – A geochronological and isotope geochemical review. *Journal of African Earth Sciences*, 46 (1-2), 93-111.
- Fleet, M.E. (2003). Rock-forming minerals, Volume 3A, Micas, second edition. *Geological Society of London*, Sheet Silicates.
- Frost, B.R., Barnes, C.G., Collins, W.J., Arculus, R.J., Ellis, D.J., Frost, C.D. (2001). A geochemical classification for granitic rocks. *Journal of Petrology*, 42, 2033-2048.
- Frost, B.R., Frost, C.D. (2008). A geochemical classification for feldspathic igneous rocks. *Journal of Petrology*, 49, 1955-1969.
- Geringer, G.J., Humphreys, H.C. and Scheepers, D.J. (1994). Lithostratigraphy, protolithology and tectonic setting of the Areachap Group along the eastern margin of the Namaqua Mobile Belt, South Africa. *South African Journal of Geology*, 97, 78-100.
- Gromet, L.P., Haskin, L.A., Korotev, R.L., Dymek, R.F. (1984). The "North American shale composite": Its compilation, major and trace element characteristics. *Geochimica et Cosmochimica Acta,* 48(12), 2469–2482.
- Jung, S., Hoernes, S., Masberg, P. and Hoffer, E. (1999). The petrogenesis of some migmatites and granites (Central Damara Orogen, Namibia): Evidence for disequilibrium melting, wall-rock contamination and crystal fractionation. *Journal of Petrology,* 40(8), 1241-1269.

- Laurent, O., Martin, H., Moyen, J. F., Doucelance, R. (2014) The diversity and evolution of late-Archean granitoids: Evidence for the onset of "modern-style" plate tectonics between 3.0 and 2.5 Ga. *Lithos*, 205, 208–235
- Macey, P.H., Siegfried, H.P., Minnaar, H. and Botha, P.M.W. (2011). The Geology of the Loeriesfontein Area. Explanation of 1:250 000 Sheet 3018 (Loeriesfontein), Council for Geoscience, 117 pp.
- Macey, P., Thomas, R., Minnaar, H., Gresse, P., Lambert, C., Groenewald, C., Miller, J., Indongo, J., Angombe, M., Shifotoka, G., Frei, D., Diener, J., Kisters, A., Dhansay, T., Smith, H., Doggart, S., Le Roux, P., Hartnady, M. and Tinguely, C. (2017). Origin and evolution of the ~1.9 Ga Richtersveld Magmatic Arc, SW Africa. *Precambrian Research*, 292, 417-451.
- Macey, P.H., Bailie, R.H., Miller, J.A., Thomas, R.J., de Beer, C., Frei, D., and le Roux, P.J. (2018). Implications of the distribution, age and origins of the granites of the Mesoproterozoic Spektakel Suite for the timing of the Namaqua Orogeny in the Bushmanland Subprovince of the Namaqua-Natal Metamorphic Province, South Africa. *Precambrian Research,* 312, 68–98.
- McDonough, W.F., Sun, S.S. (1995). The Composition of the Earth, *Chemical Geology,* 120, 223-253.
- Miller, R.M. (2012). Review of Mesoproterozoic magmatism, sedimentation and terrane amalgamation in Southwestern Africa. *South African Journal of Geology*, 115(4), 417–448.
- Moen, H.F.G. (1999). The Kheis Tectonic Subprovince, southern Africa: A lithostratigraphic perspective. *South African Journal of Geology*, 102 (1), 27-42.
- Nke, A.Y., Bailie, R.H., Macey, P.H., Thomas, R.J., Frei, D., Roux, P.L., and Spencer, C.J. (2020). The 1.8 Ga Gladkop Suite: the youngest Paleoproterozoic domain in the Namaqua-Natal Metamorphic Province, South Africa*. Precambrian Research,* 105941*.*
- Paton, C., Hellstrom, J., Paul, B., Woodhead, J., Hergt, J. (2011). Iolite: Freeware for the Visualisation and Processing of Mass Spectrometric Data. *Journal of Analytical Atomic. Spectrometry,* 26, 2508-2518.
- Pettersson, Å., Cornell, D. H., Yuhara, M., & Hirahara, Y. (2009). Sm-Nd data for granitoids across the Namaqua sector of the Namaqua-Natal Province, South Africa. *Geological Society, London, Special Publications,* 323(1), 219–230.
- Powell, R., Downes, J. (1990). Garnet porphyroblast-baring leucosomes in metapelites: mechanisms, phase diagrams and an example from Broken Hill, Australia. High-temperature

Metamorphism and Crustal Anatexis. *The Mineralogical Society Series*, Springer, Dordrecht, vol. 2.

- Raith, J., Cornell, D., Frimmel, H. and De Beer, C. (2003). New Insights into the Geology of the Namaqua Tectonic Province, South Africa, from Ion Probe Dating of Detrital and Metamorphic Zircon. *The Journal of Geology*, 111(3), pp.347-366.
- Reid, D.L. (1977). Geochemistry of Precambrian igneous rocks in the lower Orange River region. Bulletin (Ph.D. thesis), *Precambrian Research Unit*, University of Cape Town, vol. 22, 397 pp.
- Reid, D.L. (1997). Sm-Nd age and REE Geochemistry of Proterozoic arc-related igneous rocks in the Richtersveld Subprovince, Namaqua Mobile Belt, Southern Africa. *Journal of African Earth Science*s 24 (4). 621-633.
- Reid, D.L., Welke, H.J., Erlank, A.J. and Moyes, A. (1987). The Orange River Group: a major Proterozoic calc-alkaline volcanic belt in the western Namaqua Province, South Africa. In: Pharaoh, T.C., Rickard, D. (Eds.), Geochemistry and mineralization of Proterozoic volcanic suites, *Geological Society London*, Special Publication vol. 33, 327–346.
- Robb, L.J., Armstrong, R.A. and Waters, D.J. (1999). The history of granulite facies metamorphism and crustal growth from single zircon U-Pb geochronology: Namaqualand, South Africa. *Journal of Petrology*, 40, 1747-1770.
- Rollinson, H.R. (1993). Using geochemical data: evaluation, presentation, interpretation. Harlow, Essex, England: New York: Longman Scientific & Technical.
- Ronov, A.B. and Migdisov, A.A. (1971). Geochemical history of the crystalline basement and sedimentary cover of the Russian and North American platforms. *Sedimentology*, 16, 137-185.
- Sawyer, E. (2008). Atlas of migmatites. *The Canadian Mineralogist*, Special Publication 9. NRC Research Press, Ottawa, Ontario, Canada. 371p.
- Shand, S.J. (1943) Eruptive rocks, 2nd Edition, John Wiley, New York, 444p
- Streckeisen, A. (1974). Classification and nomenclature of plutonic rocks: recommendations of the IUGS sub-commission on the systematics of Igneous Rocks. *Geologische Rundschau* 63, 773–786.
- Taylor, S.R. and McLennan, S.M. (1985). The Continental Crust: Its composition and evolution, Blackwell, Malden, Massachusetts.

- Van Niekerk, H.S., Beukes, N.J. (2019). Revised definition/outline of the Kheis Terrane along the western margin of the Kaapvaal Craton and lithostratigraphy of the newly proposed Kheis Supergroup. *South African Journal of Geology*, 122(2), 187-220.
- Waters, D.J., Whales, C.J (1984). Dehydration melting and the granulite transition from metapelites in Southern Namaqualand, South Africa. Contributions to Mineralogy and Petrology, 88, 269-275.
- Waters, D.J. (1986). Metamorphic zonation and thermal history of pelitic gneisses from western Namaqualand, South Africa. *Transactions of the Geological Society of South Africa*, 89, 97-102.
- White, R.W., Powell, R., Halpin, J.A. (2004). Spatially-focussed melt formation in aluminous metapelites from Broken Hill, Australia. *Journal of metamorphic geology,* 22, 825-845.
- Winchester, J.A. and Floyd, P.A. (1976). Geochemical discrimination of different magma series and their differentiation products using immobile elements. *Chemical Geology*, 20, 325-343.

Appendix A

Weight (g) of leucosome and melanosome separates.		
Sample	**Leucosome (g)**	**Melanosome (g)**
KL 2	155.72	145.53
KL 5A	159.57	131.32
KL 6	159.42	169.04
KL 7	140.24	92.05
KL 9	155.14	58.50
KL 26	144.78	68.31
Average	152.48	110.79

Appendix B

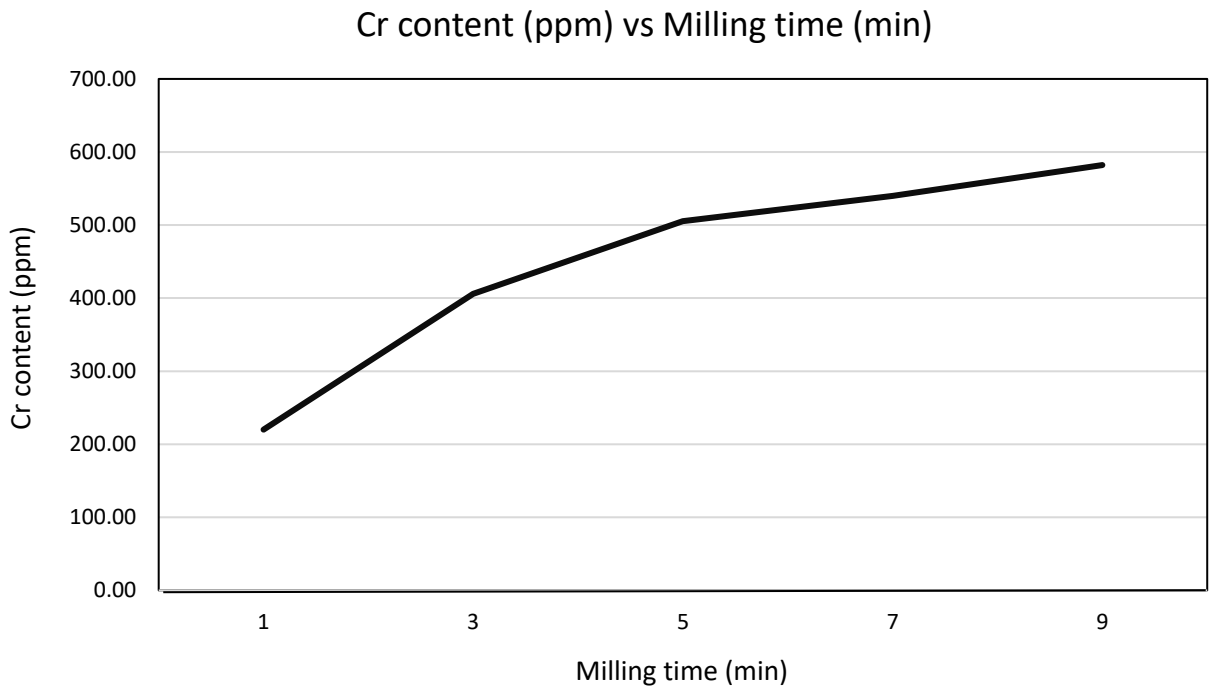

Appendix C